Research on Improvement of Propulsive Performance of a High-Speed Ship Equipped with a High-Powered Propeller

by

Yoshitaka UKON*, Kenichi KUME*, Junichi FUJISAWA*, Haruya TAKESHI**
Yasutaka KAWANAMI*, Jun HASEGAWA*, Ryohei FUKASAWA*
Shosaburo YAMASAKI***, Jun ANDO**** and Takeshi KANAI*****

Abstract

This report first describes the review results on the hydrodynamic issues on high-speed and high-powered ships and the research results for developing ship hulls and optimum propellers to concretely solve some serious hydrodynamic problems on a high-speed and high-powered ship with a large diameter single screw propeller. The discussion was made based on the research results of three-year project on "Research on Improvement of Propulsive Performance of a High-Speed Ship Equipped with a High-Powered Propeller" and the related investigation on high-speed and high-powered ships.　This project was also performed with linking to the review activities for 24th ITTC Propulsion Committee and the cooperative works between NMRI and other organizations.

The first part of the present report reviews the recent research activities for identifying the hydrodynamics issues on propulsion systems of high-powered and high-speed ships, especially large container ships.　The feasibility study reports written by the shipbuilders and researchers suggested a large container ship with the large capacity more than 10,000TEU as a future ship, including the report by the 23rd ITTC propulsion committee.　In addition this report conducts data analysis on the principal dimensions and the difficulty index based on the NMRI data and the data from the abovementioned feasibility studies on a large container ship.　The cavitation erosion and pressure fluctuations and bearing forces are identified to be the most serious hydrodynamic issues.

The second part of this report describes the improvement on the ship hulls and propellers of a high-speed and high-powered ship, such as for a large container ship.　The CFD calculations on this type of ship were carried out to confirm its usefulness.　For the present ship hull form, some difficulties were found in the grid generation near the bow and the stern to obtain reasonable solutions on the resistance and ship wake distribution.　Several ship hull forms were designed not only to reduce the wave and viscous resistance but also to make the ship wake as uniform as possible.　The stern shape modification for the wake uniformity causes the reduction of propulsive efficiency, while the reduction of wake deficit greatly reduces the pressure fluctuation amplitudes to comfortable level and erosive cavitation for the finally designed large container ship.

This report discusses the usefulness of design tools and the design results for several kinds of container ship hulls with several designed propellers through the experiments in the 400m-towing tank and the large cavitation tunnel in the NMRI.　Several propellers were designed by the respective optimum propeller design methods to reduce cavitation and the pressure fluctuations induced by cavitating propellers.　Most of the designed propellers go over the design target on the propeller efficiency, pressure fluctuations and erosion.

＊　Fluid Engineering Department, NMRI
＊＊　Center for CFD Research, NMRI
＊＊＊　Nakashima Propeller, Co. Ltd.
＊＊＊＊　Kyushu University
＊＊＊＊＊　Ship Research Center of Japan

原稿受付　平成18年11月15日
審 査 済　平成19年 8月17日

Contents

Nomenclature

A_O Propeller Disc Area (= $\pi D_P^2/4$) [m^2]
A_E Expanded Area of Propeller [m^2]
a_E Expanded Area Ratio of Propeller (=A_E/A_O)[-]
B Ship Breadth [m]
B_P Power Coefficient [-]
C Tip-Hull Clearance [m]
C_B Blockage Coefficient [-]
C_T Thrust Loading Coefficient [-]
C_{PN} Pressure Coefficient Based on Propeller Revolution Rate [-]

$$= \frac{P - P_O}{\frac{1}{2}\rho n_P{}^2 D_P{}^2}$$

$C_{0.7}$ Chord Length at 0.7R_O [m]
C_W Wave Resistance Coefficient [-]
D Depth of Ship [m]
D_P Propeller Diameter [m]
d Draft of Ship [m]
e Vapor Pressure [kPa]
Fn Froude Number [-]
F_X Axial Force [N]
F_Y Horizontal Force [N]
F_Z Vertical Force [N]
g Gravity Acceleration [m/s^2]
K, k Form Factor [-]
L_{PP} Ship Length between Perpendiculars [m]
L_{WL} Ship Length at Full Load Water Line [m]
l Lever [m]
M_X Axial Moment (=torque) [N-m]
M_Y Horizontal Moment [N-m]
M_Z Vertical Moment [N-m]
N_P Propeller Revolution Rate [rpm]
n_P Propeller Revolution Rate [rps]
P_B Brake Horse Power, BHP [kW, PS]
P_O Static Pressure [kPa]
P_P Propeller Horse Power =(η_RDHP) [kW(, PS)]
P_S Shaft Horse Power [kW, (PS)]
Rn_D Reynolds Number Based on Diameter of Propeller [-]

$$= \frac{nD_P{}^2}{\nu}$$

Rn_K Reynolds Number by Kempf's Definition at xR[-]

$$= \frac{C_{0.7}\sqrt{V_A{}^2 + (\pi x n D_P)^2}}{\nu}$$

R_O Radius of Propeller [m]
r Local Radius [m]
T Propeller Thrust [kN]
t Thrust Deduction Factor [-]
V_A Advance Speed of Propeller [m/s]
V_S Ship Speed [m/s]
w_{TM} Wake Ratio Defined by Thrust Identify Method [-]
x Non-dimensionalized Radius =r/ R_O [-]
Z Number of Propeller Blade [-]
Z_S Number of Propeller Shaft [-]

ΔF Unsteady Force Amplitude [N]
ΔM Unsteady Moment Amplitude [N-m]
ΔP_i Pressure Fluctuation Amplitude at i-th Blade Rate [kPa]
Δw Wake Deficit (= w_{max}-w_{min} or w_{max}-w_{mean}) [-]
η_R Relative Rotative Efficiency [-]
ν Kinematic Viscosity [m^2/s]
Θ Angular Position of Propeller Blade form 12 o'clock, Positive to Right Turning Direction
ρ Density of Water [kg/m^3]
σ_N Cavitation Number Based on Propeller Revolution Rate [-]

$$= \frac{P_O - e}{\frac{1}{2}\rho n_P{}^2 D_P{}^2}$$

∇ Displacement of Ship [m^3]

1. Introduction

Until now, several research projects have been proposed and feasibility studies have been conducted on high-powered and high-speed ships and their propulsion system not only in Europe and North America but also in the Far East. Among them, especially a very large container ship is a matter of concern for naval researchers, shipbuilders, ship/propeller designers, ship owners and ship operators. A large ship requires a high-powered propulsion system to absorb a big propeller torque even for a very efficient ship hull form. In this report, technical problems are reviewed on the propulsion system for high-powered and high-speed ships, and promising design and analysis tools to develop new types of ship hull forms and propulsion systems.

This report describes the review results on the hydrodynamic issues on high-speed and high-powered ships and the research results for developing optimum ship hulls and propellers to concretely solve some serious hydrodynamic problems on a high-speed and high-powered ship with a large diameter single screw propeller. The discussion was made based on the results of three-year project on "Research on Improvement of Propulsive Performance on a High-Speed Ship Equipped with a High-Powered Propeller" and the related investigation on high-speed and high-powered ships. This project was also performed with linking to the review activities on the task 6 "Review of Design Issues Related to Very Large Propellers for Mega Container Ships, such as Vibratory Forces, Cavitation and Bearing Forces" for 24th ITTC Propulsion Committee and the cooperative works between NMRI and other organizations, that is, The Ship Research Center of Japan, Nakashima Propeller, Co. Ltd., and Kyushu University.

The first part of the present report reviews the recent research activities for identifying the hydrodynamics issues on propulsion systems of high-powered and high-speed ships, especially large container ships. Ship owners and ship builders are interested in single screw large container ships with the large capacity of more than 10,000TEU for a future ship. In this report, the feasibility study reports written by the shipbuilders, ship class associations and ship consultants were investigated, including the report by the 23rd ITTC propulsion committee. Data analysis was conducted based on the NMRI data and the data from the feasibility studies to identify the principal particulars of a 12,000TEU container ship. The pressure fluctuations and erosion are identified for the most serious hydrodynamic issues.

The second part of this report describes the improvement on ship hulls and propellers for a 12,000TEU container ship. The CFD calculation was carried out to confirm its usefulness. For the present ship hull form, some difficulties were found in the grid generation near bow and stern to obtain reasonable solutions on the resistance and ship wake distribution. Several ship hull forms were designed not only to reduce the wave and viscous resistance but also to make the ship wake as uniform as possible. Although the stern shape modification for the wake uniformity causes the reduction of propulsive efficiency, the reduction of wake deficit greatly reduces the pressure fluctuation to comfortable level for the present finally designed large container ship.

This report discusses the usefulness of design tools and the design results for several kinds of container ship hulls with several designed propellers through the experiments in the 400m-towing tank and the large cavitation tunnel in the NMRI. Several propellers were designed to reduce the pressure fluctuations induced by them by several optimum propeller design methods. Most of designed propellers go over the design target on the propeller efficiency, pressure fluctuations and erosion.

2. Definition of High Speed and High Powered Ships (Minimum Requirement)

In order to survey the data on high-speed and high-powered ship, it is necessary to define the range of the target ships. This paper defines the following two terms, that is, high speed and high power.

2.1 High Speed Ship

In this paper, a high-speed ship is defined as follows,

* Ship speed V_S is higher than 22kt
* Froude number $Fn=V_S/(gL_{WL})^{0.5}$ is higher than 0.21

Both conditions should be satisfied for a high-speed ship.

2.2 High Powered Ship

In this paper, a high powered ship is defined based on published papers as follows,

* Load Coefficient $P_S\ B/(L_{PP}\ d^2 V_S^3\ Z_S)$ is larger than 0.003.
* Thrust Loading Coefficient is larger than around 1.0.

$$C_T = \frac{T}{\frac{1}{2}\rho V_A^{\ 2}(\frac{\pi D_P^{\ 2}}{4})}$$

* Power Coefficient $B_P=N_P P_P^{0.5}/V_A^{2.5}$ is larger than 18.

The above mentioned coefficients define a ship with highly loaded propeller.

* Difficulty Index $(P_S\ N_P^2)^{0.4}$ is larger than 3,500
* Difficulty Index $P_B/(\pi D_P^2/4)$ is larger than 590

All conditions together with the engine output of 100MW should be satisfied for a high-powered ship.

3. Review of Feasibility Study on Large Container Ships

3.1 Advent of Post Panamax Container Ships

In late sixties, a 700TEU (Twenty feet Equivalent Units) full-sized container ship made her debut with high light and then about half a century has passed. During this period, the ship size and the number of containers to be accommodated becomes bigger and bigger year by year. In eighties, a Panamax container ship was delivered.

In this report, a large container ship is defined as one carrying more than 4,000TEU containers and the breadth of its ship is larger than 32.24m. This is called a Post-Panamax container ship and can be designed more rationally and reasonably than the Panamax container ship whose length-beam ratio is extremely high from the hydrodynamic point of view.

In 1986, The American President lines built five Post-Panamax container ships. These C-10 type full sized container ships were built at German shipyards (HDW and Bremer Vulkan). The breadth of the ship is 39.4m and this ship carried 4,340TEU containers. The containers were stowed twelve wide in the hold and sixteen wide on the deck. The maximum output of the main engine reached 41.9MW at 95rpm for 85% MCR with 20% sea margin. Propeller design, powering and prediction of pressure fluctuations were important tasks for the designers of ship and propeller. Additionally, not only propeller strength and shaft force due to the heavy weight but also hull vibration response were big problems. The thrust-loading coefficient C_T of this ship was estimated to be around 0.9. The pressure fluctuation amplitudes at full scale were measured 7～9kPa at her sea trial.

After 1995, 5,000TEU container ship appeared and recently large container ships which carry a 5,000～8,000TEU containers were built. In 1996, a Super Post Panamax container ship appeared. The Maersk Line built the L-type container ship “Regina Maersk” at the Ordense Shipyard and then the ship size rapidly became larger and larger. The overall length and the breadth of this ship were 318.2m and 42.8m. Containers are stowed 14 wide in the holds and 17 wide on the decks of the vessel. This ship carried 6,250TEU nominally. Since no detailed information on this ship was published, the load factor and others were unknown.

Nowadays major ship owners have plans to build ultra-large container ships carrying 10,000～13,000TEU containers. A 7,500TEU container ship, “Hamburg Express” was delivered in October 2001. Several 9,500TEU container ships were ordered in 2003.

3.2 Feasibility Studies on Large Container Ships

Around the end of twentieth century, the universities [1), 2)], ship model basins, the classification associations [3)], shipbuilders and ship owners carried out feasibility studies and conceptual ship and propeller design studies on mega container ships. A number of articles on naval architect magazines were issued on the present topics. In this section, recent argument on mega container ships at the symposium on “Mega-Container Ships in Future” organized by the Kansai Society of Naval Architects, Japan [4)-8)] and recently published related reports and papers are reviewed.

3.2.1 Design Results by KHI（Kawasaki Heavy Industry, Co.）

Based on the existing 5,250TEU container ships built by KHI, 7,000TEU and 7,900TEU container ships were designed [5)]. In the case of a single propeller shaft ship, propeller designers face serious cavitation problems, especially on propeller blades and a rudder. To avoid detrimental cavitation, a propeller must be designed with the blades of large expanded area ratio. On a 5,250TEU container ship, the wave resistance at 25kt amounts to 20% of total resistance. The reduction of wave resistance for such big container ships is one of the most important tasks for hull form designers.

The maximum output of an existing low speed Diesel engine is 70MW up to now, but 120MW Diesel engine is technically feasible by increasing the number of the cylinders and its bore pressure. The propeller shaft can bear 110MW power. The ship speed of 25kt should be kept for the container ships to make a weekly service. Even if bigger engines than the existing one can be produced, the draft limitation due to harbor depth is still big barrier for its propeller designer. The larger expanded area of the propeller becomes, the worse propeller efficiency is given. The single screwed propeller for large container ships could not be designed without the loss of propeller efficiency. The KHI suggested that few problems on the propulsion system and engine are expected except the increase of the building cost and fuel consumption if these types of ships equip with twin screws.

3.2.2 Design Results by IHI（Ishikawajima-Harima Industry, Co.）

IHI announced the development of a new contra-rotating propeller system for 4,000～10,000TEU Post Panamax container ships [6)]. Assuming to equip one of the existing engines to the ships, the conventional single screw propulsion system can be applied for less than 8,500TEU container ships sailing at 25kt with 20% sea margin, while the new contra-rotating propeller system can be applied for

10,260TEU container ships. The maximum output of the main engine was assumed to be 65.9MW at 100rpm. This ship is expected to save 12% of the engine output, comparing with that equipped with a normal single screw propeller and single engine.

When contra-rotating propellers are applied to such a large container ships, the design of bearings for propeller shafts becomes more difficult and the occurrence of erosive vortex cavitation stems from the blades of a forward propeller to those of a rear one can be suspected, because the relative tip speed of such a large diameter propeller is extremely high.

3.2.3 Design Results by Lloyd's Register

The Lloyd's Register made extensive investigation into the design problems on five kinds of Post Panamax container ships from 4,000TEU to 12,500TEU and reported the conceptional design results and the discussion in detail [7), 8)]. Detailed useful data and information to predict ship and propeller performance were also included in the report [8)]. In order to examine the feasibility of ship speed from 23 to 25kt for a 12,500TEU container ship（L_{PP}=381m, B=57m, D=29m, d=14.5m）and to clarify the design problems, the study designs were performed. It is confirmed that this size of the ships can stow 12,500TEU containers by 18 wide in holds and 22 wide on the deck and by arranging the main deck house at the midship.

In the Lloyd's Register's reports, four options of propulsion system, one propeller by one engine, twin propeller by two engines (the propeller shaft are installed in gondola skeg), contra-rotating propellers (CRP) and one propeller plus one podded propeller were compared. The merit and demerit were discussed for each ship. It is expected that a normal CRP system have problems on the bearing of propeller shafts at the stern. One propeller plus one podded propeller have problems on unsteady cavitation occurrence and bearing force under the steering condition of a podded propeller.

If an available low speed diesel engine of 81MW at MCR was equipped as a main engine with 25% sea margin for a normal single screwed container ship, the ship speed of 25kt can be obtained for 8,800TEU but only 23.5kt can be achieved for 12,500TEU container ship. To obtain the ship speed of 25kt, twin screw and two engines should be applied for more than 9,000TEU container ships. In this case, not only the ship price but also the service costs unacceptably increase. The ship speed of 25kt for a 12,500TEU container ship with a single propeller by one engine requires a 98MW engine and a six-bladed propeller with 9.8m in diameter and expanded area ratio of 1.03. The weight of the propeller made of NiAl Br amounts to 129ton, and technical problems on the propeller manufacturing reveal.

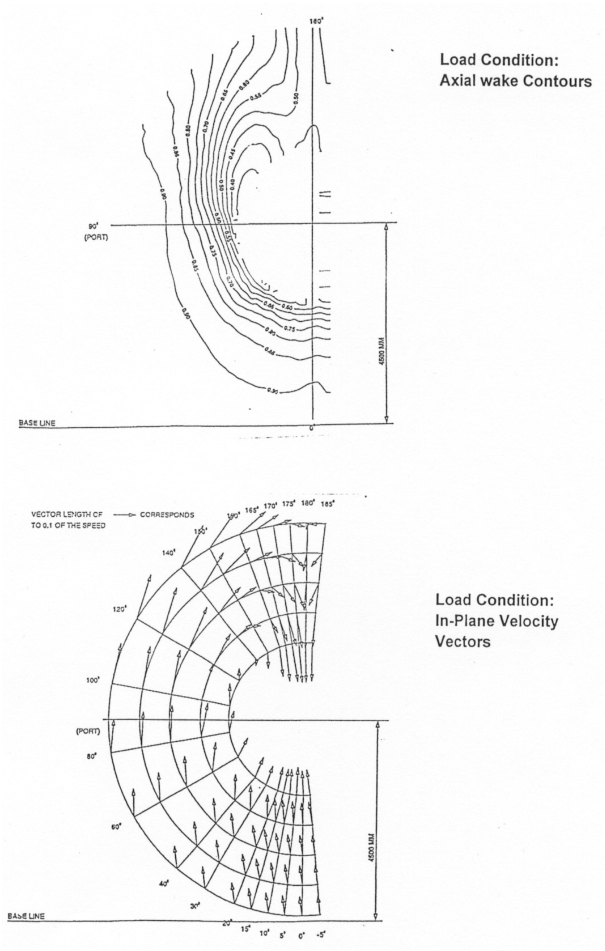

Fig. 3.1 Wake Distribution of a Typical Panamax Container Ship (from Reference 7 or 8)

A typical axial and in-plane, radial and circumferential wake distribution for a 6,500TEU container ship are shown in **Fig. 3.1**. The bigger the wake deficits, Δw, that is, the difference between the maximum wake and the minimum wake or the mean wake during one revolution, the higher the pressure fluctuation amplitudes. The wake deficits relate to the derivatives of wake variation in the vicinity of the top position, that is, 12 o'clock position where the propeller blades pass. In the case of higher pressure fluctuations than acceptable level, life cycle on the fatigue of stern hull structure and hull resonance and forced vibration become serious problems.

In the Lloyd's Register's reports, an estimation chart on the first blade rate of hull surface pressure amplitude is shown for three cases of wake deficits from 0.2 to 0.4 against the nominal TEU capacity as shown in **Fig. 3.2**. In this figure, the wake deficits are defined as the non-dimensional velocity difference between the mean effective wake and the maximum one. This figure suggests acceptable wake deficits within normally expected range of hull surface pressure level.

The circumferential wake component affects on the growth and collapse of unsteady propeller cavitation. The computational and experimental prediction methods give us an appropriate guidance to predict the first blade rate of pressure fluctuations and cavitation extent on the propeller blades. On the other hand, no reliable prediction methods on the higher harmonics than the first blade rate of hull surface pressure fluctuations exist except the model experimental one at present.

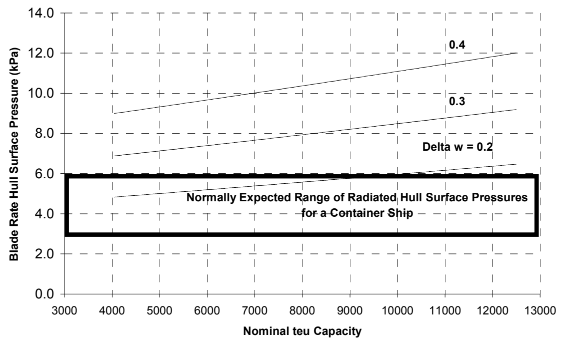

Fig. 3.2 Chart of Predicted Pressure Fluctuations (from Reference 8)

The propeller tip speed is one of the most important parameters to predict the onset and development of propeller cavitation. For mega container ships, the tip speed of the single screwed propeller becomes 49～59m/s and cavitation occurrence can not be fully avoidable around the propeller tip. Then, the cavitation should be kept to be stable under control and the occurrence of tip vortex cavitation bursting, face cavitation and cloud cavitation must be completely prevented. In order to avoid the occurrence of unsteady cavitation due to the slope of circumferential wake variation, the adoption of a highly skewed propeller is effective but not always.

3.2.4 Design Results on World's Largest Reefer Container Ships

Recent development of the propeller design procedures and propulsive data including self-propulsion factors and full form information are described in detail for a large innovative reefer container ship, "Dole Chile" [9]. Since the service speed is 21kt and the transportable capacity is 2,000TEU, this ship should be classified as a moderate Full-Panamax container ship.

The propeller designers aimed at the best balance on high propulsive efficiency, low hull pressure fluctuation level (less than 3.5kPa) and favorable maneuverability. The propeller design was made three times starting from the original moderately skewed propeller with 35.5degree skew, changing the skew distribution and the diameter by using HSVA propeller design program codes. The design results were evaluated by the computational program codes on propeller performance and cavitation prediction and confirmed by the model experiments at the HSVA large cavitation tunnel, Hykat. Cavitation extent on the designed propeller blade observed in the model tests became less than that on the previous one and was improved at each design step. Since the used computational method underpredicted the cavitation extent on the designed propeller, it might be suggested that the current computational design tools work well qualitatively but should be improved.

The full-scale measurements on pressure fluctuations were performed at the engine output of 20MW and the propeller revolution rate of 97rpm. The single pressure amplitude at the first blade rate was 2.6kPa and kept within the requirement of "Comfort class level". The cavitation test results with a complete ship model at Hykat agreed well with the full-scale measurements, while the computational method predicted slightly higher values than the full-scale data in this case.

3.3 Review by The 23rd ITTC Propulsion Committee

In the report of the 23rd ITTC Propulsion Committee [10], the difficulty in propeller design on mega container ships was discussed as one of the most important tasks. This committee report indicated several issues on the propeller design as follows. The propulsive power became 100MW per shaft and an equipped propeller had usually six blades. The expanded area ratio should be larger than 0.9 and the diameter of propellers were used in the range of more than 8.75m. These propellers were driven by a slow speed, two-stroke Diesel engine and operated at the propeller revolution rate around 100rpm. The circumferential tip speed is usually larger than 45m/s and the thrust loading coefficients C_T are around 1.0. The design margins of propellers for this class are extremely small and the propeller design can be made successfully only for favorable or homogeneous wake distribution. The hydrodynamic computational and experimental design and prediction tools are still needed. It has been required to predict the absolute level of pressure fluctuation induced by propeller and cavitation and the risk of cavitation erosion accurately. Nevertheless, few reliable computational prediction methods exist especially on the absolute level of pressure fluctuation amplitudes induced by unsteady propeller cavitation.

The 23rd ITTC Propulsion Committee indicated that the design of 25kt and 90MW single screwed container ship for 10,000TEU would be feasible but highly sophisticated design tools and simultaneous / concurrent design are inevitable for this case.

3.4 Data Analysis from Published Data

This section describes concrete data analysis results especially on the propeller thrust loading, difficulty index and pressure fluctuation for several classes of container ships including mega container ships, using the data obtained from the naval architect magazine and papers in several related symposium proceedings. In order to investigate how critical the propeller design for mega container ships is, rough data analysis was performed on the "Difficulty Index" proposed by 23rd ITTC propulsion committee [10] and others, such as the thrust-loading coefficient and hull surface pressure level. The following container ships are selected from published data and NMRI data of its own projects as the objects of examination. The principal dimensions and other information of ships and propeller, and the used values for analysis are shown in **Table 3.1**.

Since some of the necessary data on a ship hull form and propulsive data, such as effective horsepower, thrust deduction coefficient, wake coefficient, were not given clearly, they should be suitably estimated. Propellers were designed by using several MAU propeller charts. The design point of propeller was determined from a given ship speed and main engine output. For the data from sea trials and full-scale measurements, the sea margin was noted to be zero as shown in **Table 3.1**.

(1) Principal Dimensions

First of all, the tendency of principal dimensions for container ships is examined. The plots of the ship length between perpendiculars, L_{PP} are roughly linear to the capacity of containers as shown in **Fig. 3.3**. Then, Froude numbers decrease from 0.26 to 0.21, corresponding to the increase of container capacity.

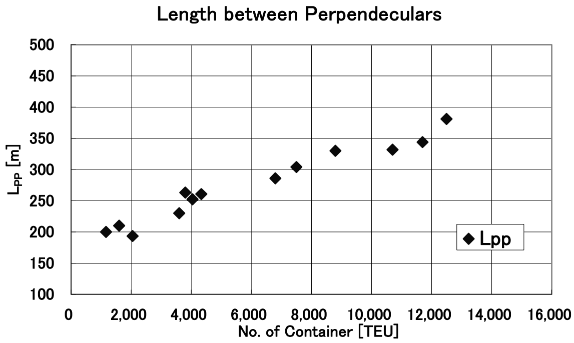

Fig. 3.3 Relation between Container Capacity and Ship Length

The length-breadth ratios L/B of concerned container ships are shown in **Fig. 3.4**. They are around 7, while the breadth/length draft ratios L/d are roughly proportional to the container capacity and range from 3 to 4. The former tendency might be affected by the draft restriction in the container yard and the harbor.

Table 3.1 Principal Particulars and Analyzed Results for Containerships

TEU		1,166	1,600	2,046	3,600	3,800	4,340	7,500	4,040	6,800	8,800	10,700	12,500	11,699
DWT	[ton]	22,936						100,000						
Loa	[m]	213.00	225.83	204.90		275.00	275.00	320.38						362.00
Lpp	[m]	200.00	210.00	193.40	230.00	263.00	260.80	304.00	252.40	286.00	330.00	332.00	381.00	344.00
B	[m]	29.00	30.50	32.24	32.20	32.20	39.40	42.80	37.30	42.80	45.60	55.10	57.10	48.00
d(Design)	[m]	10.52	11.00	9.23	10.80	11.50	10.98	13.00	12.20	12.70	13.00	13.40	13.80	17.00
L/B	[-]	6.90	6.89	6.00	7.14	8.17	6.62	7.10	6.77	6.68	7.24	6.03	6.67	7.17
B/d(Design)	[-]	7.34	7.40	6.36	0.00	8.54	6.98	7.49	0.00	0.00	0.00	0.00	0.00	7.54
C_B(Design)	[-]	0.5784	0.6168	0.6619	0.6505	0.6384	0.5573	0.6774	0.6020	0.6230	0.6250	0.6280	0.6300	0.6140
MCR	[kW]	25,166	23,001	23,924	39,100	35,909	41,711	68,640	65,354	74,475	83,118	108,713	131,666	100,045
Np(MCR)	[rpm]	101.0	111.9	97.0	115.0	101.4	95.0	94.0	123.6	118.4	120.5	123.1	126.8	101.3
S.M.	[%]	15.0	0.0	0.0	20.0	0.0	0.0	15.0	25.0	25.0	25.0	25.0	25.0	20.0
VS	[kt]	22.40	22.00	21.50	24.00	25.00	24.00	25.30	25.00	25.00	25.00	25.00	25.00	25.00
Fn(Lpp)	[-]	0.2603	0.2495	0.2540	0.2600	0.2533	0.2442	0.2384	0.2586	0.2429	0.2261	0.2255	0.2105	0.2215
Admirality Coefficient	[-]	679.0	745.4	577.4	672.4	826.9	601.1	874.5	658.9	725.6	764.7	708.3	667.5	731.0
Dp	[m]	7.40	7.000	7.00	7.900	7.85	8.400	9.10	8.400	8.850	9.200	9.500	9.800	10.400
$D_P/d_{\_Des}$	[-]	0.703	0.636	0.758	0.731	0.683	0.765	0.700	0.689	0.697	0.708	0.709	0.710	0.612
CT w/o S.M.	[-]	0.815	1.026	1.051	1.027	0.819	0.912	0.900	0.840	0.885	0.896	1.204	1.485	1.217
$(MCR*N_P^2)^{0.4}$	$[PSrpm]^{0.4}$	2,612	2,736	2,479	3,458	3,020	3,045	3,685	4,499	4,579	4,852	5,496	6,074	4,547
$MCR/(\pi D_P^2/4)$	[kW/m²]	585	598	622	798	742	753	1,055	1,179	1,211	1,250	1,534	1,746	1,178
DI		7.2	9.1	2.4	7.2	9.2	10.6	10.6	6.5	8.3	10.7	16.7	22.6	28.6
ΔP(Estimate)	[kPa]	5.62	5.51	3.41	7.80	7.18	7.97	6.58	10.66	10.79	12.03	13.30	14.93	10.40

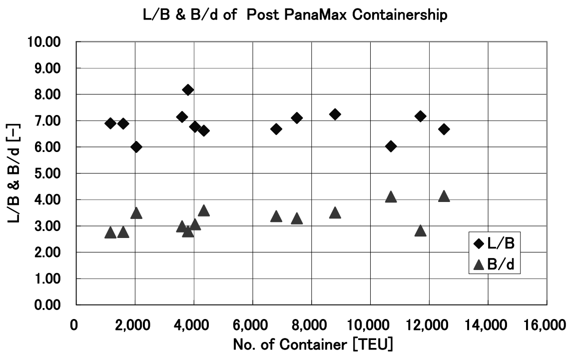

Fig. 3.4 Relation between Container Capacity and Length/Beam and Beam /Draft Ratio

Since a few data on the blockage coefficient C_B or the displacement of ships can be usually found in the literature, the container ships discussed here are selected from those whose C_B are known or clearly described. As shown in **Fig. 3.5,** C_B ranges from 0.58 to 0.70 and is independent on the increase of container capacity.

As shown in **Table 3.1**, the propeller diameter-draft ratio is around 70% for single screwed ships, from the viewpoint of prevention of propeller racing and this relation was used as standard criteria.

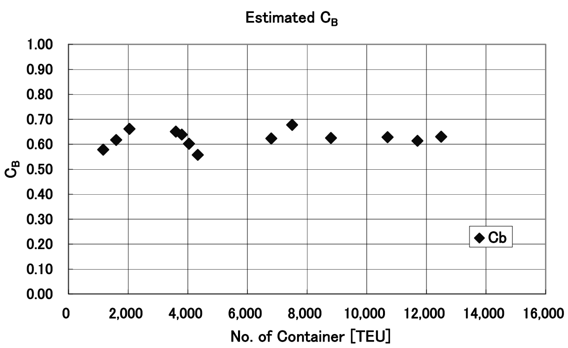

Fig. 3.5 Relation between Container Capacity and Blockage Coefficient

(2) Propeller Thrust-Loading

Since the propeller efficiency depends on the propeller thrust-loading coefficient C_T and the type of propeller, the thrust-loading coefficient is one of the most important parameters in the propeller design and indicates the difficulty in the propeller design. For these container ships, the propeller thrust-loading coefficients are estimated by assuming the propeller diameter from the criteria mentioned above, if the diameter is not described.

The respective propellers were designed using several MAU propeller charts. The propeller efficiency and expanded area ratio were determined by these charts. The estimated thrust-loading coefficients shown in **Fig. 3.6** are constant and about 1.0 for the container ship less than 10,000TEU, while the thrust loading coefficients increase to 1.5 with the increase of container capacity.

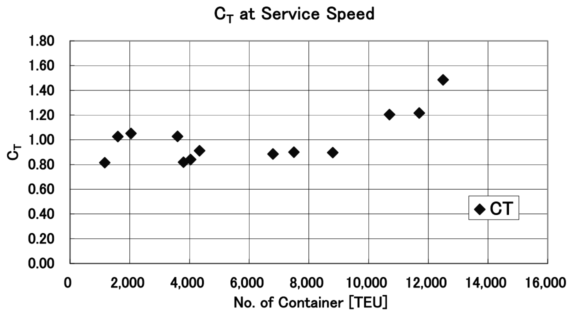

Fig. 3.6 Relation between Container Capacity and Thrust Loading Coefficient

For such a high thrust-loading coefficient condition, the design of propeller becomes more difficult. It is feared that not only the excessive cavitation occurrence on the propeller blades but also the thrust breakdown might not be avoided for the ships with the container capacity more than 10,000TEU due to the high speed of ships.

(3) Difficulty Indexes

Several “difficulty indexes” have been proposed for high-speed and high-powered ships as described in the previous section. The 23rd ITTC Propulsion Committee recommended the following difficulty index DI derived from systematic series of experiments at MARIN on single screwed container ships

$$DI = \frac{T \cdot N_P{}^2 \cdot \Delta w^5 \nabla^{3/4}}{5 \cdot 10^7 \cdot Z \cdot \dfrac{A_e}{A_O} \cdot \sqrt{C}}$$

The Propulsion Committee recommended that the DI should be less than 7 as the tentative upper limit from the viewpoint of the maximum allowable hull excitation level. These difficulty indexes are estimated for the container ships described in **Table 3.1** and the results are shown in **Fig. 3.7**. Most of difficulty indexes are larger than the recommended value by the 23rd ITTC and show us the difficulty in propeller design for this class of ships. Especially for larger than 10,000TEU container ships, the present difficulty indexes become tremendously large even up to about 30. They cannot be used for the expected giant containerships simply but are effective to improve the ship hull form and propeller as a measure.

The wake deficits are most predominant to the ITTC difficulty index, DI. For mega container ships, the uniformity of ship wake is decisive to design a "Less-Cavitation Propeller" successfully within allowable hull excitation level. This index, however, should be applied carefully for other kinds of ships. It becomes too small, if applied to propellers for a RoPax ferry. The tendency of rapid increase in the DI against the container capacity larger than 10,000TEU is similar to that of the thrust-loading coefficient C_T as shown in **Fig. 3.6**.

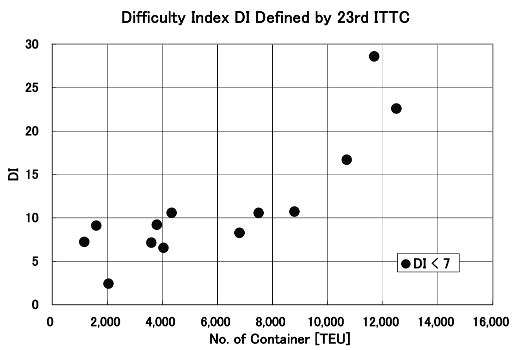

Fig. 3.7 Relation between Container Capacity and 23rd ITTC Difficulty Index

Other difficulty indexes $(P_B N^2)^{0.4}$ or P_B/A [11] are shown in **Fig. 3.8**. Both data linearly increase with the increase of container capacity. Roughly speaking, the former values are larger than the upper limit against the container capacity more than 5,000TEU. This index is also effective to express the design difficulty for mega container ships. Since all of the latter values are beyond the upper limit, this index is not recommendable for the use of this class of ships.

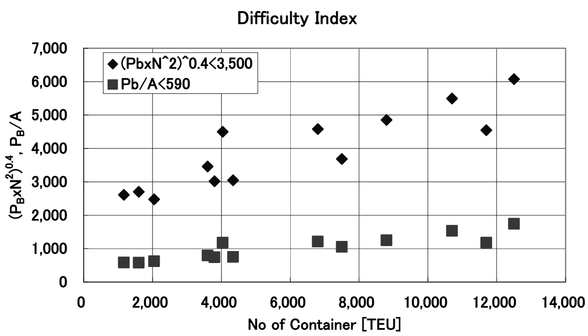

Fig. 3.8 Relation between Container Capacity and Other Difficulty Indexes

(4) Hull Surface Pressure

The estimated hull surface pressure amplitudes at the first blade rate for the container ships are shown in Table 3.1 and calculated by a "simplified Holden Method". The results are shown in **Fig. 3.9**. For the ships with more than 8,000TEU of container capacity, extraordinarily high amplitudes of pressure fluctuations are predicted larger than 10kPa and most of the plots made are far beyond the maximum allowable level of 6kPa. Lower pressure fluctuation amplitudes for the 7,500TEU and 11,700TEU container ships are expected due to the lower propeller revolution rate and the larger draft, respectively.

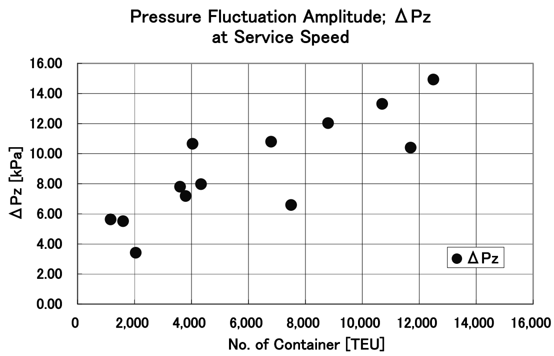

Fig. 3.9 Relation between Container Capacity and First Blade Rate Pressure Amplitudes

3.5 Review for The 24th ITTC Propulsion Committee

3.5.1 Survey on Recent Trend on Large Container Ships

The 24th ITTC Propulsion Committee distributed the questionnaires with the following four questions to Korean and Japanese shipyards [12]. Four Japanese and four Korean shipyards replied to the questions.

(1) Recent building record on large (more than 4,000TEU) container ships.
(2) Principal particulars of the propellers and the engines, propeller diameter, number of blade, engine power, propeller revolution rate and difficulty index.
(3) Any experience and potential problems on cavitation, erosion, hull pressure, bearing force of large container ships.
(4) Ongoing research project, future plan, papers, reports related to mega container ships.

Several replies to the questions (1) and (2) on main engine power, propeller diameter, number of blades and propeller revolution rate against the container capacity (TEU) are summarized and some of these are shown in **Figs. 3.10 and 11**. The main engine power is linearly proportional to the capacity of containers as shown in **Fig. 3.10** and reaches the maximum of currently available ones, 68.6MW of the largest two strokes diesel engine with 12 cylinders for 9,000TEU container ships.

For a 12,000TEU future container ship, the engine power is predicted 100MW to keep the required service speed of 26kt and should be designed by 18 cylinders [13), 14)]. Larger container ships should run faster than smaller ones to offer a competitive container line service and to recover longer time loss during the container loading [13)].

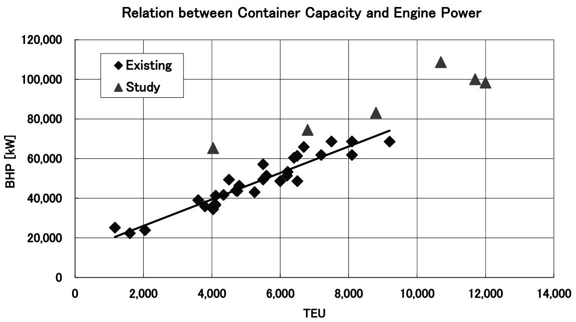

Fig. 3.10 Trend on Main Engine Power of Current Container ship

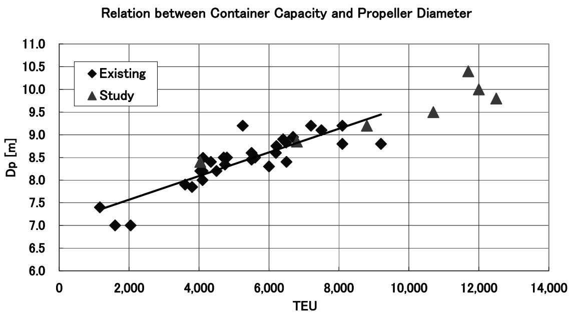

Fig. 3.11 Trend on Propeller diameter of Current Container ship

The number of propeller blade becomes six for the large container ship more than 8,000TEU. **Fig. 3.10** also predicts 100MW engine for 12,000TEU container ships. The propeller diameter increases with the increase of the container capacity as shown in **Fig. 3.11**, while the upper limit around 10m exists because of the restricted ship draft determined by harbor depth. The maximum scantling draft is set to 14.5m for the container ships more than 6,000TEU and the design draft is assumed from 13.0m to 13.8m. The propeller diameter is usually determined 70% of the draft due to the propeller immersion under the ballast conditions [8), 13), 14)].

The propeller revolution rate remains constant between 95 and 100rpm.

3.5.2 Potential Problems on Mega Container Ships

Some potential problems for single mega-container ships are discussed in the previous committee report. By referring to the replies to the question (3) mentioned above and the discussions in the review papers and the feasibility study reports, the following potential problems might be suggested. No experiences on propeller cavitation problems are reported from the Japanese and Korean shipyards.

＊ Engine power; supply of engine (more than 68.6MW), engine accommodation (length)
＊ Propulsion system selection [13), 15), 16)]; single screw, twin screw, normal single screw with pod propulsor, CRP, performance prediction.
＊ Hull design [8), 13), 14)]; generation of high quality lines, reliable NFD (Numerical Fluid Dynamics is defined as numerical tolls including potential theories, such as the boundary element method) and optimization technique, wake uniformity, large propeller tip clearance, high propulsive efficiency, less wave and pressure resistance.
＊ Propeller design; selection of diameter and number of blade, accomplishment of target propeller efficiency, determination of blade strength and thickness, design without thrust break-down, propeller boss and cap design, tip and hub vortex cavitation and cloud cavitation suppression.
＊ Hull vibration; quantitative prediction, higher order pressure fluctuations, prevention of bursting of propeller tip vortex cavitation, prevention and reduction methods of vibration [16), 17)].
＊ Propeller cavitation erosion; prediction by NFD and experiment, suitable trailing-edge shape with anti-singing treatment, understanding of bubble collapse process and mechanism of intensive impact pressure emission.
＊ Rudder cavitation; rudder gap cavitation, rudder shape design (size, profile, section), rudder cavitation prediction by NFD and experiment, prediction of erosion.
＊ Bearing force; accurate prediction including that under turning conditions, determination of shaft diameter, design of resultant force at stern tube bearing due to the shaft forces and the propeller weight including that at low revolution rate.
＊ Experimental technique; development of experimental techniques using small models due to large scale ratio, wake simulation including full scale wake simulation and its prediction, Reynolds and Froude effects, model-ship correlation.

* Propeller manufacturing; weight, transportation (size), material, casting, repair technique.
* Maneuvering; prediction of maneuverability, turning ability, stopping ability.
* Stability; parametric rolling.
* Economical benefit; oil price, global economical growth.
* Social infrastructure; harbor depth, capacity of container birth, crane capacity, road or transportation capacity.

Among the potential problems mentioned above, the optimum design of a propeller and a hull form including a rudder might be picked up as one of the most important design issues. Since a highly powered propeller for large container ships induce big bearing forces and surface forces, the establishment of reliable prediction methods for both forces is still needed.

3.5.3 Design Issues for Very Large Single Screw Propellers

Wake Uniformity

In order to design a very large propeller for mega container ships successfully, optimum hull form design to create a uniform flow is inevitable. The 23rd ITTC committee proposes the difficulty index DI and as the tentative upper limit the DI related to the maximum allowable excitation level of 7 is given [10), 18)]. The difficulty index seems to be useful at the preliminary design stage. The difficulty index is given as follows.

The wake deficit, Δw is one of the most predominant parameters in this equation because of 5th power. Other parameters, tip clearance, thrust and blade number are not so crucial except the propeller revolution rate. The optimum hull form design to produce fine uniform wake and the large tip clearance is very important items for the propeller design.

The present committee sent the additional questionnaire to the Japanese and Korean shipyards to investigate the usefulness of the DI defined above and to clarify the real DI based on the large container ship built and delivered recently. Based on these data together with additional existing data, the difficulty indexes versus the container capacity TEU are plotted and they scatter along 0.0013×TEU ± 4 as shown in **Fig. 3.12**. The upper limit of the real DI might be suggested 12.0. In the case of the DI equal to about 17, not plotted in this figure, unfavorable design problems are reported.

Since it is most effective to reduce the wake peak value of the wake deficit, the optimum hull form design by NFD is expected to give a possible solution to the design issues for large propeller together with optimization techniques, that is, GA (genetic algorithm), Neural Network and so on. 10% reduction of the wake deficit offers 41% reduction of the difficulty index. The difficulty index of the 12,000TEU container ship is predicted as 15.6 by the approximation equation in this figure, while the recent trend indicates the lower difficulty index than the predicted value by this equation. By improving the wake distribution and stern hull form drastically, 12,000TEU container ships might be feasible, if the difficulty index can be controlled less than 12.

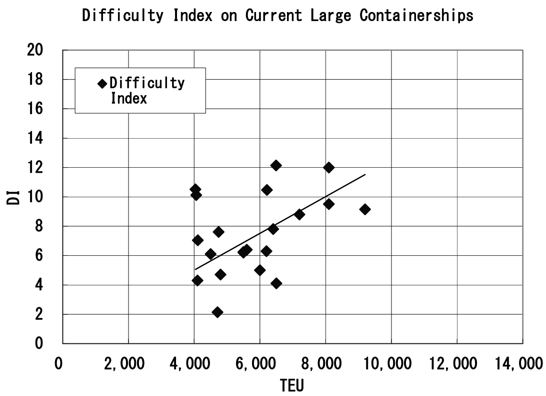

Fig. 3.12 Relation between Container Capacity and 23rd ITTC Difficulty Index

Cavitation Appearance

To concretely demonstrate the hydrodynamic aspect of a mega container ship propeller, a ship model was manufactured and self-propulsion test and cavitation test using a complete ship model were performed [14), 19)]. For the design speed of 26kt with 20% sea margin, the main engine power to be installed was estimated around 100MW. The propeller diameter is determined 10m for the design draft of 14.5m.

Fig. 3.13 Cavitation Pattern on Large Propeller of a Mega-Container Ship under MCR ($\sigma_{N\_0.8R}$, Θ=30deg)

Pressure fluctuation measurements on a six-bladed prototype propeller without skew in an estimated full scale wake show very high pressure amplitude level and the first blade rate amplitude which is predominant to other blade rates is estimated as around 11kPa at the tip clearance of 28% diameter under the MCR condition. Therefore, the cavitation experiment on a large diameter propeller should be performed by using the cavitation number defined at a suitable radial position considering the head effects on the static pressure of propeller blades, such as $0.8R_O$.

Fig. 3.13 shows foaming type cavitation pattern and erosive cavitation were observed at the vanishing stage of unsteady cavitation, while no signature was found from the results of the paint erosion test. One of the reasons why the paint was not removed off might be small tip speed in the cavitation model test. The development of quantitative experimental prediction method should be recommended.

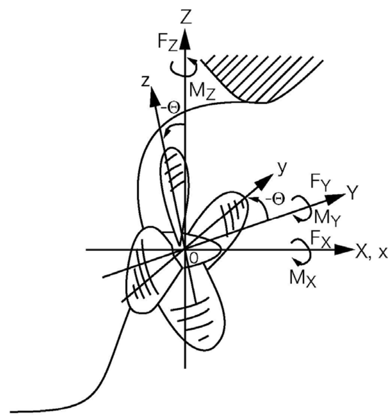

Fig. 3.15 Definition of Coordinate System on Bearing Force

Bearing Force

Based on the estimated full scale wake [14), 19)] for this ship by Sasajima and Tanaka's method as shown in **Fig. 3.14**, bearing forces are predicted by several propeller performance analysis programs currently used in Japan and Korea. The weight of six-bladed propeller with the diameter of 10m is assumed 120ton in the air.

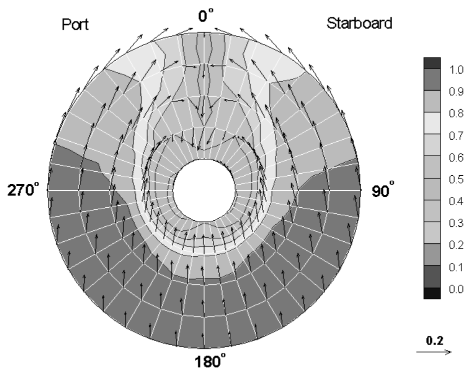

Fig. 3.14 Estimated Full Scale Wake Distribution of a Typical Post-Panamax Mega-Container ship

The coordinate system is defined in the present computation as shown in **Fig. 3.15**. Since the comparative computations were performed in 12th ITTC, no survey on the prediction accuracy level for the bearing force has been carried out during more than thirty years. In the previous comparative computation, steady (averaged) component was not discussed in detail.

In 24th comparative computation, the bearing forces were evaluated by introducing the equivalent forces F'_Z or F'_T calculated from the computed bending moment M_Y or M_Z as shown in **Fig. 3.16**. In the present comparative computations, the cavitation effects on the propeller performance including the bearing force were neglected.

Seven Japanese and one Korean organizations took part in the 24th ITTC comparative computation on the bearing force. They are Ishikawajima-Harima Heavy Industry, Co. (IHI), Kyushu University, Mitsubishi Heavy Industry, Co. (MHI), Mitsui Engineering and Shipbuilding, Co. (MES), Nakashima Propeller, Co. (Nakashima), National Maritime Research Institute (NMRI), Samsung Heavy Industry, Co. (Samsung) and Sumitomo Heavy Industries Marine & Engineering, Co., Ltd. (Sumitomo). Each has its own computer program code to design propellers or to make safety regulation and others. Most of them have good experience on building large container ships and/or large propellers.

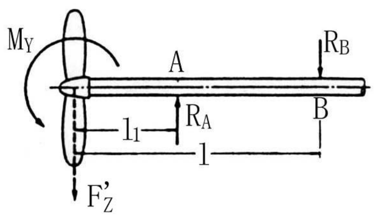

Fig. 3.16 Concept for Computing Equivalent Force from Bending Moment

Using the same input data, the six-component bearing forces were computed by their currently used methods. NMRI and Nakashima computed the bearing forces by the mode function type of unsteady lifting surface theory program codes developed by Koyama, K. [20)] (NMRI) and Yamasaki, S. (Nakashima) [21)], respectively. MHI, Sumitomo and Kyushu University employed own unsteady lifting surface program code based on the Quasi-Continuous Method (QCM) developed by Hoshino, T. (MHI) [22)], Streckwall, H. (HSVA) [23)] and Ando, J. (Kyushu University) [24)], respectively, to compute the bearing forces. MES and Samsung calculated the bearing forces by each unsteady vortex lattice program code developed by Ishii, N. (MES) [25] and Lee, C.-S. [26], respectively. IHI predicted the bearing forces by using a quasi-steady propeller blade theory based on van Manen's induced camber method [27].

The predicted results on the fluctuating and the steady components are shown in **Figs. 3.17 (a)** and **(b)**, respectively. The fluctuating components of bearing force in **Fig. 3.17 (a)** seem to be relatively small, while the steady component of predicted vertical bending moment M_Y, in **Fig. 3.17 (b)** is unfavorably big, which might cause bearing troubles. In addition, the data scatter in the vertical bending moment prediction might be so big that bearing and shaft specialists cannot judge whether the vertical force at the bearing is acceptable or not. The prediction methods should be improved especially on the steady component and the validation with experiments is necessary..

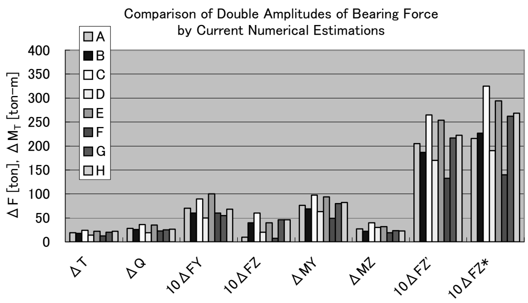

(a) Fluctuating Components

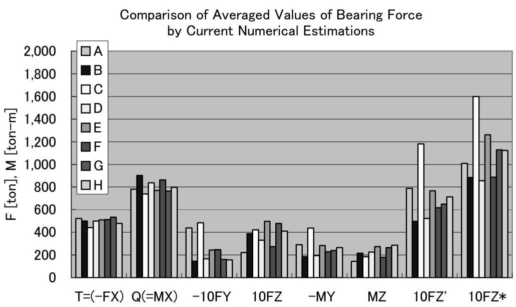

(b) Steady Components

Fig. 3.17 Comparison of Numerical Prediction Results on Bearing Force for 12,000TEU Container ship

In order to reduce unsteady cavitation and pressure fluctuations, the circumferential wake uniformity during one revolution of a propeller is decisive. This uniformity requirement also reduces such a big upward force equivalent to the propeller weight and adjusts the moderate load at the rear end of stern tube bearing. Since the scatter of estimated values on bearing force, especially the vertical force F_Z and the vertical moment M_Y, is too big, the improvement of numerical bearing force estimation technique should be required from the view point of the bearing and shaft design.

It is recommended that the resultant vertical force including an equivalent force converted from the vertical bending moment at the propeller center should be estimated roughly less than 50% of the propeller weight and the scatter of the prediction should be within 25% of the weight. Nevertheless, the predicted resultant vertical force F_Z* by the present computations scatters from 73% to 134% of the propeller weight and the deviation corresponds to 35% of the weight.

The resultant forces are defined as,

$$F_Z{}^* = F_Z + F_Z{}'$$

$$F_Y{}^* = F_Y + F_Y{}'$$

In this situation when the upward force is equivalent to the propeller weight, then the resultant side force becomes more predominant. Since the downward force at the bearing becomes the maximum under the dead slow turning condition because the weight of the propeller and shaft is the only load acting the bearing, the design of bearing becomes more critical.

3.6 Concluding Remarks from Review

Further effects on the development of a new concept of hull form are needed to make more uniform wake inflowing into the highly powered propeller blades and to design the angles of attack as low as possible, especially in the vicinity of the stern hull. On the other hand, the development of a "Less-Cavitation Propeller" is required to reduce the pressure fluctuations on the stern hull. The propeller blade section devised from the concept of flat pressure distribution is not feasible and sometimes brings worse results. A flow-adapted propeller is more promising to manage the pitch and local load distribution along the propeller radial direction circumferentially [i. e. 10)].

As other options, a contra-rotating propeller and a tandem propeller might be cited. The former propeller has a fear of cavitation erosion, while the latter propeller might have a problem on bearing force due to the weight of a propeller and propeller efficiency. A sophisticated optimum design method has not developed on tandem propeller yet.

4. Improvement of Propulsive Performance of a Large Container Ship

4.1 Introduction

From the review results on the recent research on high-speed and high-powered ships, it is concluded that the hydrodynamic design issues on single screwed large container ships should be investigated as one of the research items. The 24th ITTC Propulsion Committee was also assigned to review the design issues related to very large propellers for mega container ships, such as vibratory forces, cavitation and bearing forces.

Reflecting these circumstances, the present research project focused on the concrete demonstration of the design issues on a large container ship with systematic experiments and paid attention to the improvement of propulsive performance on the large container ship equipped with a large single screw propeller.

Shipbuilders and propeller designers have improved the ship hull form and optimized the propeller in their design to the requests by ship owners year by year. Recently high-speed and high-powered ships cause several hydrodynamic problems explicitly, such as erosion and ship vibration.

As a target ship in the present research, a 12,000TEU class container ship was selected. This report discusses what kinds of hydrodynamic issues are important and serious for single screwed mega container ships with more than 10,000TEU container capacity. It is said that this size of container ship is difficult to design with existing ship building technology [5), 6)]. It also seeks for effective design and prediction tools to improve the performance of ship hull and propulsor and to make such mega container ships with a single screw possible as one of the targets for this research project.

This paper primarily describes the design challenge on the large diameter propellers for the large container ships.

4.2 Prototype Ship Hull and Propeller

4.2.1 Design of Ship Hull

First of all, the prototype of ship hull was designed for a large container ship with referring to current feasibility studies [3), 8)], and the Japanese port authority information. The principal dimensions were roughly determined by the University of Michigan's estimation method [3)] on the accommodation of capacity containers.

The over all length of ship is 362.0m and the breadth of ship hull is 56.3m with considering the berth availability (maneuverability in a berth and crane outreach). The design draft for the prototype is 14.49m due to the depth restriction of the new berth of Yokohama container terminal.

In this paper, the required engine power is assumed 100MW at 100rpm. This size of two-stroke low-speed engine has not been developed until now but a motor with 18 cylinders could be available and offer a brake horsepower of 103MW [13)] in the near future. The design speed of the prototype is assumed to be 25.0kt with 20% sea margin with taking into account the new trend for the ship hull.

Table 4.1 shows the principal particulars of the prototype ship. The ship length between the perpendiculars was determined to be 344m based on the trends in the survey work described above, as shown in **Fig. 4.1**. L/B and B/d of the present ship hull are 6.11 and 3.9, respectively. These are within the range of the expected future large container ships given in the section of the review. The blockage coefficient is also in the range between 0.58 and 0.68.

Table 4.1 Principal Particulars of Original and Prototype Ship

Original & Prototype Ship (Scale Ratio=50)			Full Scale Size	
			M.S. No.728	M.S. No.732
Bow Shape			Conventional Bulb	High Bulb
Stern Shape			Conventional	
Length between P.P.	L_{PP}	[m]	344.00	
Length at Load Water Line	L_{WL}	[m]	354.00	
Breadth	B	[m]	48.00	56.30
Draft (Design)	d_{Design}	[m]	17.00	14.49
Depth	D	[m]	29.00	
Propeller Shaft Height	H_{SC}	[m]	5.30	

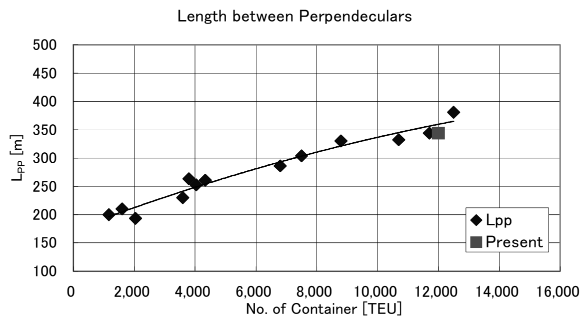

Fig. 4.1 Trend in Ship Length for Large Container Ships

The lines of the prototype hull form were generated by the SRC method of hull form optimization based on Neural Network [28)]. The bulbous bows equipped to the original and prototype ships are shown in **Fig. 4.2**. The ship model, NMRI M. S. No. 732 was manufactured by wood and equipped with the studs for turbulence stimulation at the square station, S.S. 9.5 and at the middle of the bulbous bow. Resistance tests, self-propulsion tests and wake measurements on the several ship models (including M. S. No. 732) were conducted in the NMRI 400m towing tank. The photo of ship wave around the model of a prototype ship is shown in **Fig. 4.3**.

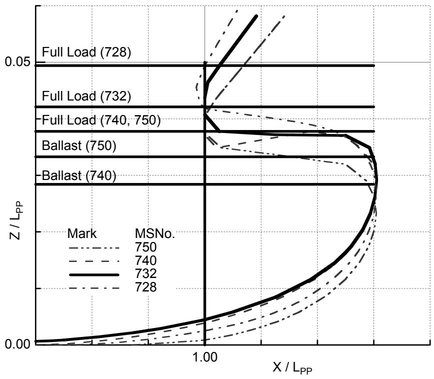

Fig. 4.2 Comparison of Bulbous Bows for Tested Container Ships

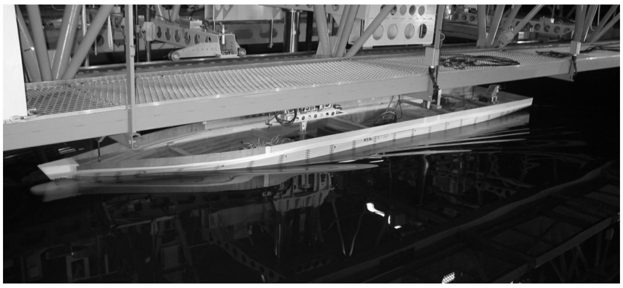

Fig. 4.3 Ship Wave around M. S. No. 732 at Froude Number Equivalent to 26.0kt

4.2.2 Performance of Ship Hull

(1) Experiment

From resistance on M. S. No. 732 at 25kt (Fn=0.2183) under the full load condition, the form factor 1+k and the wave resistance coefficient $C_W x10^3$ are 1.16 and 0.132, respectively. The effective horsepower is 43,881kW (59,921PS). From the self-propulsion test, the self-propulsion factors, 1-t, 1-w_{TM} and η_R are 0.853, 0.715 and 1.012, respectively. The propeller loading coefficient is 0.986 for the propeller diameter of 10m. The wake ratio in full scale 1-w_S is assumed to be 0.779.

At 26kt (Fn=0.2271) under full load condition, $C_W x10^3$ of this ship is 0.150 and the effective horsepower is 50,125kW (68,150PS). 1-t, 1-w_{TM} and η_R are 0.850, 0.717 and 1.013, respectively. The thrust loading coefficient is 1.002. The propeller efficiency is 0.668 and the propulsive coefficient is 0.737. The delivered horsepower is 68,051kW (92,523PS). From the powering results, the installed engine is estimated 100MW (135,962PS) for this ship.

The wake measurement on this ship model was carried out to generate the estimated full-scale wake for the cavitation test and to examine the wall effects on the wake behind complete ship models in the NMRI cavitation tunnel. The measured results are shown in **Fig. 4.4**.

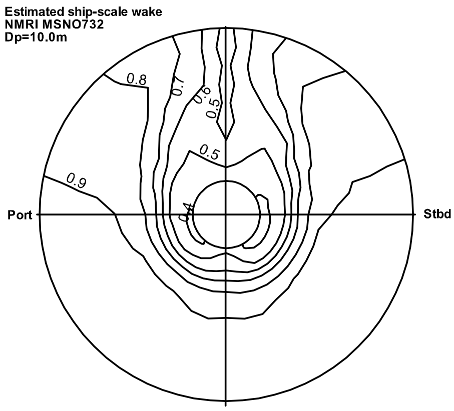

Fig. 4.4 Model Wake Distribution on M.S. No. 732 Measured in the 400m Towing Tank

(2) CFD

The Computational Fluid Dynamics (CFD) analysis is expected to be used as a practical tool to predict the flow field around complex configurations, such as a ship with a working propeller and a rudder. In this research, the effort was made to employ the CFD tools for improving the ship hull. First of all, in order to confirm the usefulness and applicability of the CFD codes developed at NMRI, the flow computations of large container ships were made and compared with the experimental data[29),30)] performed in the NMRI towing tank.

To obtain the turbulent flows around the ship models, M.S.No.728 and 732, the NEPTUNE (Newton-relaxation scheme for Pseudo-compressibility based on Turbulent Navier-Stokes Equations) code[31)] was used. This code is based on a structured grid and solves the three-dimensional Navier-Stokes equations with the artificial compressibility based on a cell-centered finite-volume formulation. The inviscid fluxes are evaluated by the Roe scheme and MUSCL extrapolation is adopted to attain the third order accuracy, while the viscous fluxes are centrally differenced. The equations are solved by an approximate Newton relaxation method with a symmetric Gauss Seidel iterative approach. The code can employ the multi-grid and local time stepping techniques to accelerate the convergence to a steady solution. The nonlinear free-surface conditions are implemented and the interface fitting method with a re-griding technique is used to treat the free-surface deformation.

The CFD computations were carried out for the original ship hull, M. S. No. 728 and the prototype ship hull, M. S. No. 732. The former ship has a conventional bulbous bow and its draft is 17.0m in full scale, while the latter has the high bulb and shallower draft than the former as shown in **Fig. 4.2**.

In the present computations, the detailed shape of the stern tube was simplified and the transom stern is approximated as a curser type stern to obtain the converged solution efficiently. The computational grid is constructed with H-O topology. The number of grid points is 145 (longitudinal direction) x 33 (girth direction) x 97 (normal direction to the hull surface) as the standard. The minimum grid spacing in the normal direction is $1\text{-}2\times10^{-6}$ L_{PP}. The solution domain is ranged from $1\times L_{PP}$ upstream of F.P. to $2\times L_{PP}$ downstream of A.P.

The resistance of the original ship (M. S. No. 728) was calculated to validate the used CFD code by the comparison with the experimental data. The turbulence model used is Baldwin-Lomax model. On this ship, a reasonable agreement on the form factor 1+k between the experiment and the computed result is observed as shown in **Fig. 4.5**. The computed wave resistance values C_W are also demonstrated in this figure, which over-estimate the measured data, may be due to the stern shape modification. The possible reason to be considered is a poor approximation of the transom stern shape. To round off the sharp edge of the transom stern is essential for practical uses and further investigation is required.

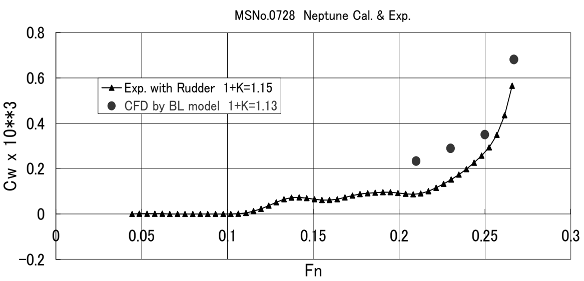

Fig. 4.5 Comparison of Wave Resistance and Form Factor between CFD Prediction and Experiment for M.S. No.728

In the wake computation, y- and z- symmetries are considered about the vertical and horizontal planes to minimize computer resources. The grid is body fitted to facilitate the implementation of boundary conditions and is clustered near the ship hull, z- and y-symmetry planes.

The computed wake distribution at $x/L_{PP}=0.98$ for M. S. No. 728 by the present code under the double model condition are compared with the measured one in the towing tank at the designed Froude number Fn=0.21 as shown in **Fig. 4.6**. The Reynolds number of the computation is set at 4.0×10^{6}. As a turbulence model, the modified Spalart-Allmaras model was used for the wake computation. The round shape of measured axial velocity contour curves is not reproduced well with the present computation. This is partly because the stern tube is not modified in the computation.

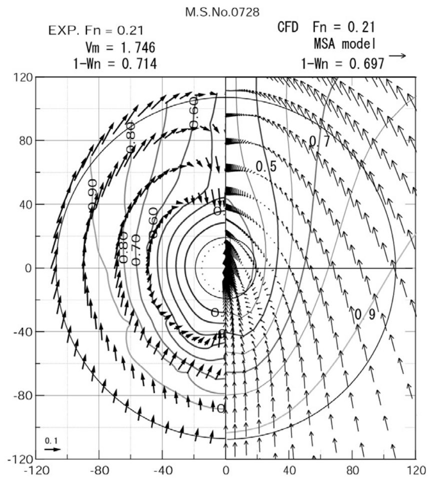

Fig. 4.6 Comparison of Wake Distribution between CFD Prediction and Measurement for M.S. No.728

4.2.3 Design of Propeller

The diameter of the prototype propeller was determined 10m, which is less than 70% of the design draft of the ship hull to avoid propeller racing phenomena. The number of the propeller blade was six as usual.

Based on the self-propulsion test data, the prototype propeller was designed by the MAU design chart for six-blade propeller and Burrill's chart for determining the expanded area ratio. The design condition on the ship speed was changed from 25kt to 26kt at normal operating rate of the engine (NOR), because the larger the container ships become, the faster they should sail from port to port to maintain acceptable schedules and to be competitive to smaller ones.

Table 4.2 Principal Particulars of Prototype Propeller

M.P. No.			047	575	576
Diameter (Full Scale)	D_{PS}	[m]	10.030	10.000	
Diameter (Model)	D_{PM}	[m]	0.2006	0.2000	
Boss Ratio	x_B	[-]	0.1800		
Pitch Ratio at 0.7R	$P_{0.7}$	[-]	1.013	0.9800	0.9300
Exp. Area Ratio	a_E	[-]	0.6340	0.6400	0.7700
Skew Angle	Θ_S	[deg]	8.2	8.3	10.0
Rake Angle	κ	[deg]	5.0		
Number of Blade	Z	[-]	6		

The principal particulars of model propellers are shown in **Table 4.2**. On this propeller, the difficulty in the design of propeller was examined. At first, the thrust loading coefficient C_T was calculated and shown in **Fig. 4.7** together with the analyzed data on the large container ships described in the previous chapter. As demonstrated in **Fig. 4.7**, the trend of C_T is around 1.0 in the range less than 10,000TEU and increases rapidly larger than 10,000TEU. C_T for the present propeller is 0.98 at the design ship speed of 26kt and not so large due to relatively large diameter of the prototype propeller.

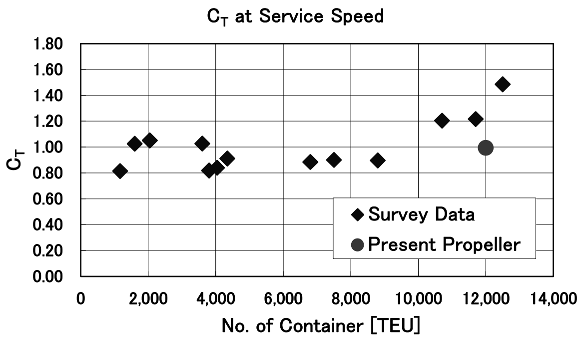

Fig. 4.7 Thrust Loading Coefficient for the Prototype Ship

The 23rd ITTC difficulty index for this ship and propeller was examined and plotted in **Fig. 4.8**. The difficulty index for the present ship became 29.5, while the recommend index by the 23rd ITTC Cavitation Committee is lower than 7.

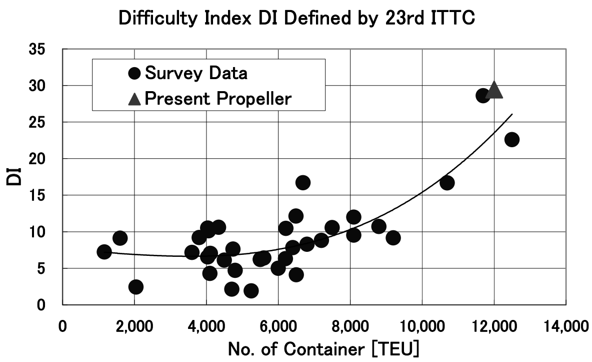

Fig. 4.8 Difficulty Index for the Prototype Ship

Finally, the power density was checked for the prototype propeller. This index is defined as follows,

$$PD = \frac{P_B(MCR)}{\left(\dfrac{\pi D_P{}^2}{4}\right)}$$

The power density of this propeller is 887kW/m^2 and less than the anticipated value in the literature [13)], because of the larger diameter of the propeller. The tip speed of the propeller is expected to reach 53m/s and the occurrence of cavitation is unavoidable.

4.2.4 Cavitation Performance

In order to investigate the cavitation performance of the prototype propeller equipped to the prototype ship hull, the cavitation experiments were performed in the NMRI large cavitation tunnel using the complete ship model.

(1) Wake Simulation

In advance of the cavitation tests, the wake measurement by five-hole Pitot tube and the simulation both for the full scale and the model were carried out using two kinds of the flow liners. Since the No. 2 measuring section of the NMRI cavitation tunnel is not huge, the wall effects on the wake distribution behind the complete ship model are not negligible generally. The model wake equivalent to the measurements in the towing tank was simulated by employing the No. 1 (small size) flow liner, while the estimated full scale wake was made by No. 2 (medium size) flow liners. The respective position of the flow liners was varied with the wake simulation to get acceptable wake distribution.

The measured wake (Rn= 1.1x10^7) in the towing tank is shown in **Fig. 4.4**, while the estimated one based on the measurements in the towing tank and the computations of the potential flow around this ship model is shown in **Fig. 4.9**.

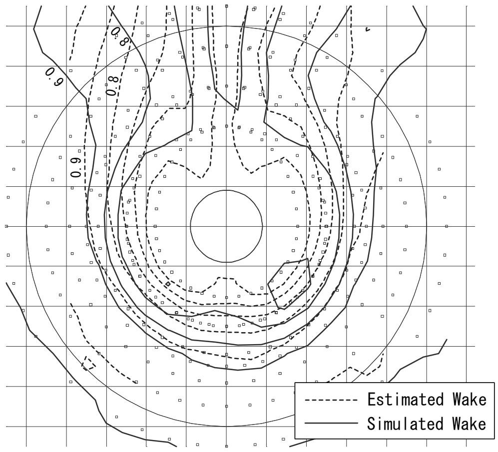

Fig. 4.9 Comparison of Estimated and Simulated Wake in the Cavitation Tunnel

The viscous wake of the full-scale ship was estimated from that obtained by the potential components by subtracting from the measured model wake. This prediction method proposed by Sasajima and Tanaka[14)] assumes that the viscous wake width is proportional to the square root of the ratio of two friction coefficients. The simulated wake distributions for the model (Rn=1.1x10^7) and for the full-scale (Rn=3.8x10^9) are shown in **Figs. 4.10** and **4.11,** respectively.

The wake breadth of the latter is narrower than that of the former and the wake peak of the latter wake is lower than that of the former.

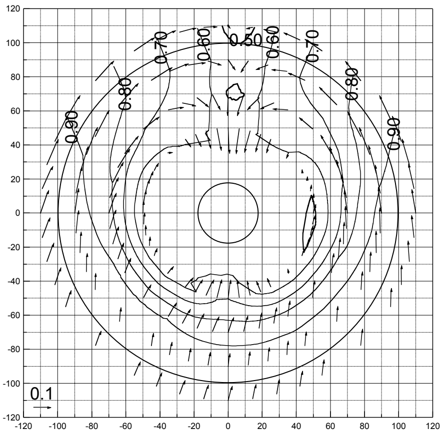

Fig. 4.10 Simulated Model Wake Distribution for Prototype Ship (M.S. No. 732)

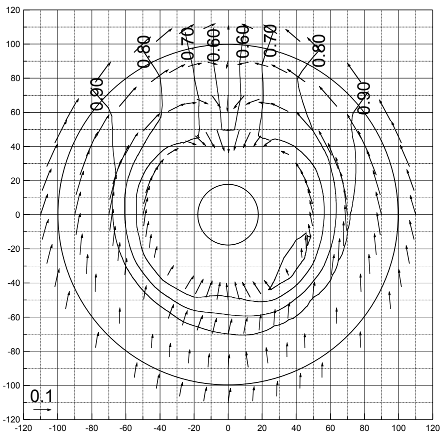

Fig. 4.11 Simulated Full-Scale Wake Distribution for Prototype Ship (M.S. No. 732)

(2) Measuring Devices

The propeller performance was measured by the propeller dynamometer (K&R R46, T_{max}=70kgf, Q_{max}=4kgf-m, n_{max}=33.3rps). To measure the unsteady pressure induced by propeller and cavitation, seventeen pressure gauges (Kyowa Dengyo, PS-2KM) were employed and equipped to the ship model hull surface above the propeller not only in the longitudinal but also transverse directions as shown in **Fig. 4.12**.

A hydrophone (B&K 8103) was equipped as the acoustic center of the hydrophone coincided to the propeller disc. The underwater sound pressure levels were measured by a hydrophone.

The ship hull was equipped with stainless steel wires at the Square Station (S.S.) 2 to supply the hydrogen bubbles and to stimulate cavitation inception in the case of insufficient cavitation nuclei distribution in the tested water.

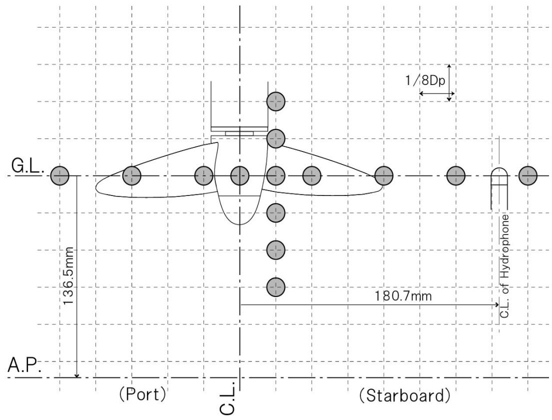

Fig. 4.12 Arrangement of Pressure Gauges and Hydrophone

(3) Experimental Condition

The experimental conditions, especially the thrust coefficient K_T or the thrust loading coefficient C_T are shown in **Table 4.3** and were given by the powering results for the maximum continuous rate (MCR) and the normal operating rate (NOR) of the engine. The cavitation number was defined by the static pressure at the shaft center and 80% radius at the upright position. At the several cavitation numbers for 80% radius position at MCR ($\sigma_{0.8R\_MCR}$), for 80% radius position at NOR ($\sigma_{0.8R\_NOR}$) and for the shaft center at MCR (σ_{SC_MCR}), the cavitation experiments were performed.

Table 4.3 Experimental Conditions

Condition		MCR (0.8R)	MCR (S. C.)	NOR (0.8R)
Engine Output		MCR		85%MCR
BHP (w/o 20% SM)	[MW]	82.7		70.3
	[PS]	112,498		95,623
Loading Condition		Full Load		
Thrust Loading Coefficient	C_T	1.016		0.9929
Thrust Coefficient	K_T	0.1908		0.1887
Definition of Cavitation Number		at 0.8R above S.C.	at S.C.	at 0.8R above S.C.
Propeller Revolution Rate	N [rpm]	95.0		90.2
Cavitation Number	σ_N	1.151	1.491	1.276

(4) Cavitation Appearance

From the results of cavitation test on the prototype propeller model, M. P. No. 576 working behind the complete ship model under the conditions of $\sigma_{0.8R\_MCR}$ and σ_{SC_MCR}, sheet cavitation initiates from the blade angular position of 340deg under both conditions, while the cavity extent under σ_{SC_MCR} was smaller than that under $\sigma_{0.8R\_MCR}$ and half of the latter. This suggests that the selection of cavitation number is decisive to simulate the cavitation patterns for such a large diameter propeller suitably. The cavitation patterns under both conditions at the blade angular position of 30deg are compared in **Fig. 4.13**. The cavity under the σ_{SC_MCR} disappeared at 50deg and 10deg earlier than that under $\sigma_{0.8R\_MCR}$. Unfavorable cavitation patterns were observed under $\sigma_{0.8R\_MCR}$.

In the desinent stage, the sheet cavity under each condition disappeared in bubbly and foam type as shown in **Fig. 3.13**, and slight erosion was anticipated on the propeller blades. The paint erosion test using "Aotak paint" was performed during 30minutes. No removed-off paint was found at all. It is said that the erosion intensity and erosion rate increase in proportion to sixth power of velocity and third power of scale. The present erosion test can not predict erosion in the full scale due to small scaled model in spite of the occurrence of unfavorable cavitation pattern. Under all of experimental conditions, no face cavitation was observed. Hub vortex from this propeller was thick, while the tip vortex was gentle.

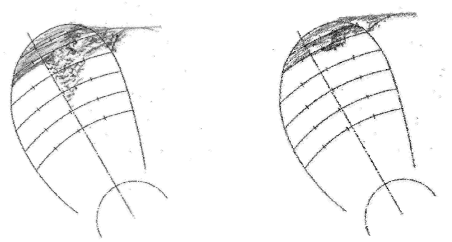

(a) MCR (0.8R) at 30deg (b) MCR (S.C.)

Fig. 4.13 Comparison of Cavitation Pattern on M.P. No. 576 between Different Cavitation Number Definitions

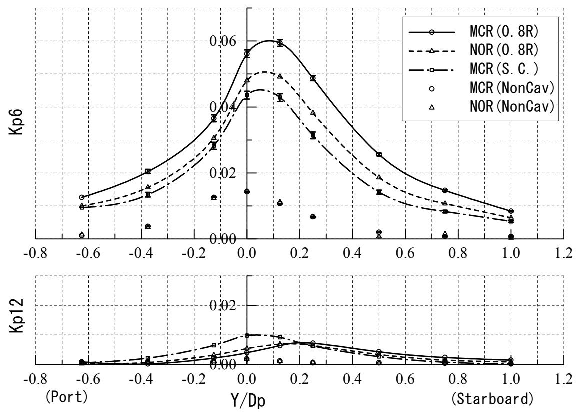

Fig. 4.14 Measured Pressure Fluctuation Amplitudes Induced by the Prototype Propeller (M.P. No. 576) Working behind the Prototype Ship Model (M.S. No. 732)

(5) Pressure Fluctuations

On very large container ships, extremely large pressure fluctuations were predicted by a simplified prediction method as shown in **Fig. 3.9**. The measured pressure fluctuation amplitudes at the first and second blade rates on the complete ship hull above the prototype cavitating propeller, M. P. No. 576 were measured under several experimental conditions in the NMRI cavitation tunnel. The measured results are shown in **Fig. 4.14**.

Under the non-cavitating condition for M. P. No. 576, the non-dimensionalized amplitude at the first blade rate was 0.015, while under the MCR at cavitation number at 0.8R, it became 0.060 and extraordinarily high in the estimated full-scale wake. In the model wake, it became higher than 0.070. The pressure fluctuation amplitude under the former working condition amounts to 15.4kPa in the full-scale ship and this level of the pressure fluctuations is not acceptable without discussion. This measured value is plotted in the estimation chart for the pressure fluctuation at first blade rate as shown in **Fig. 4.15**.

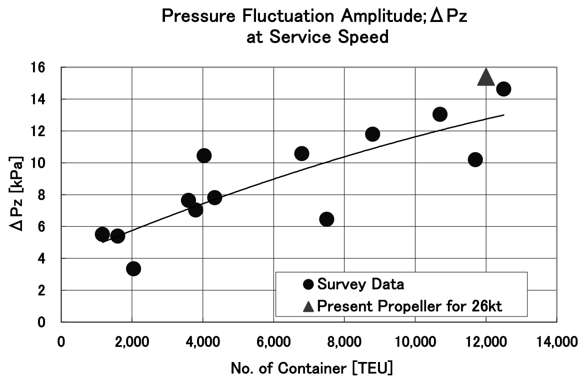

Fig. 4.15 Comparison of Measured Pressure Fluctuations on the Present Prototype with Other Data

Several reasons for such high pressure fluctuations can be indicated as follows. One of them is too large diameter due to large design draft of the prototype ship. Another is too small tip clearance of $0.23D_P$. The other is the adoption of the MAU propeller with a constant pitch distribution, small skew and non-optimum blade section. From the cavitation test using the complete ship model, it is concluded that the stern shape should be modified to make the wake more uniform and to realize larger tip clearance.

4.3 Improved Ship Hull and Propeller

4.3.1 Design of Ship Hull

It is suggested that the prototype ship hull form and propeller offer tremendous ship hull vibration. In order to reduce the pressure fluctuations to acceptable level, that is, less than 6 kPa, the hull form design to reduce the required power and the optimum propeller design to increase the propeller efficiency and to reduce the cavitation extent are needed. From reviewing the design condition of the present large container ship from the feasibility studies, the design draft was changed from 14.5m to 13m, taking into account the scantling draft of 14.5m. The installed engine was assumed 95MW including 20% Sea Margin and for the design speed of 26.0kt.

To reduce the wave resistance, the nose-up bulbous bow was adopted for this ship in place of a cylindrical bulbous bow. The lines design was carried out based on the SRC method for hull form optimization to determine the height and length of the bulb as shown in **Fig. 4.2**.

On the other hand, the stern shape was also improved to get sufficient tip clearance and horizontal screw aperture as shown in **Fig. 4.16**.

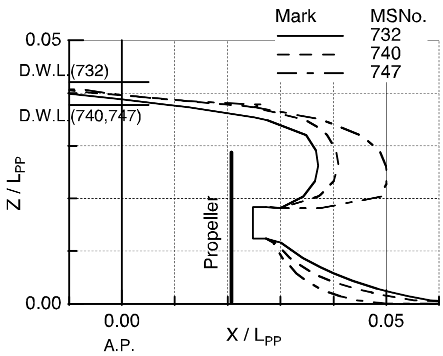

Fig. 4.16 Comparison of Stern Shape

With proportion to the decrease in the design draft, the propeller diameter was changed from 10.0m to 9.8m. The overhang part of stern hull just above the propeller was shifted upward. To addition, the “semi tunnel stern” shape with concave hull surface was adopted as shown in **Fig. 4.17**.

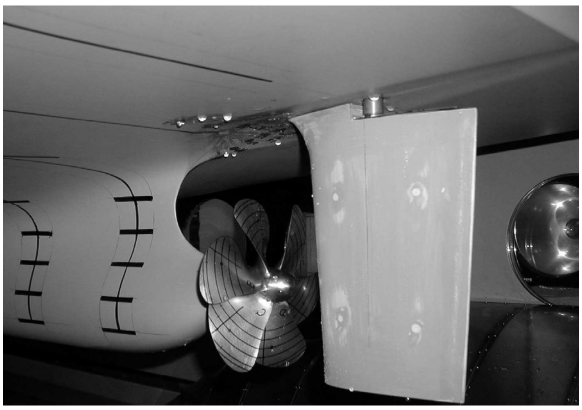

Fig. 4.17 “Semi Tunnel Stern” for Improved Ship, M. S. No. 740

Then the tip clearance increased from $0.23D_P$ to $0.35D_P$. In order to make the wake field more uniform, the stern frame from above the shaft line was shifted to the stem and the stern bulb sectional area was increased and the gravity center of the area was made lower. The principal particulars of the improved ship model are shown in **Table 4.4**.

Table 4.4 Principal Particulars of Improved Ship

Improved Ship (Scale Ratio=48)			Full Scale Size	
			M.S. No.739	M.S. No.740
Bow Shape			Nose-Up Bulb	
Stern Shape			Low Bulb	Semi Tunnel
Length between P.P.	L_{PP}	[m]	344.00	
Length at Load Water Line	L_{WL}	[m]	336.90	334.83
Breadth	B	[m]	55.50	
Draft (Design)	d_{Design}	[m]	13.00	
Draft (Scantling)	d_{Scant}	[m]	14.50	
Depth	D	[m]	29.00	
Propeller Shaft Height	H_{SC}	[m]	5.00	

The wake distribution measured at 400m towing tank of the improved ship hull, M. S. No. 740 is shown in **Fig. 4.18**.

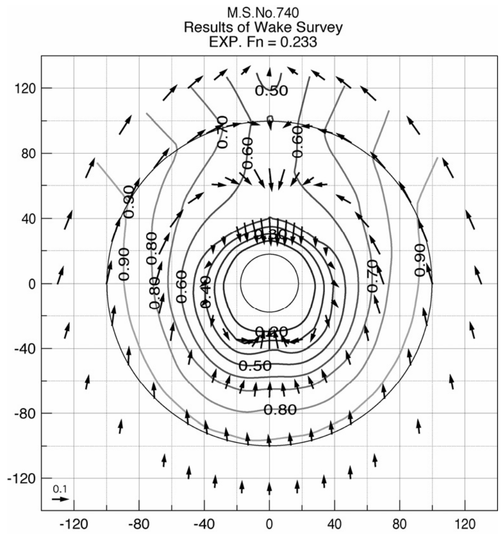

Fig. 4.18 Measured Wake Distribution behind Improved Ship, M. S. No. 740

4.3.2 Performance of Ship Hull

(1) Experiment

Using the manufactured ship model made of wood, the resistance and self-propulsion tests and the wake measurement were conducted at the 400m towing tank. Under the design full load condition, the form factor 1+k and the wave resistance coefficient C_W x10^3 at 26kt (Fn=0.2328) are 1.225 and 0.059, respectively.

The effective horsepower EHP at 26kt is 47,038kW (63,954PS) and 5.5% less than that of the prototype ship.

The self-propulsion factors for D_P=9.8m, 1-t, 1-w_{TM} and η_R are 0.839, 0.698, 1.042, respectively. The thrust loading coefficient is 1.047. The propeller efficiency is 0.616 and the propulsive efficiency is 0.708. The delivered horsepower is 66,440kW (90,333PS) and 2.3% less than that of the prototype ship.

(2) CFD

The NEPTUNE code was first applied for the computation of the resistance and the flow field around the improved ship hulls with the nose-up bulbous bow, M. S. No. 739 and 740. No satisfactory and consistent solutions were obtained even by the computational efforts with changing the geometrical draft (Z/L_{PP}=0) to the computed draft of Z/L_{PP} =0.023. The reason why the artificial draft was applied for this computation is the difficulty in the grid generation above the nose-up bulb due to the large skewness as shown in **Fig. 4.19** and due to the application of the structured grid.

However, it turned that the structured grid approach of the NEPTUNE code encounters difficulties in the grid generation above the nose-up bulbous bow, since there is little space between the bulb top and the water surface as shown in **Fig. 4.19**.

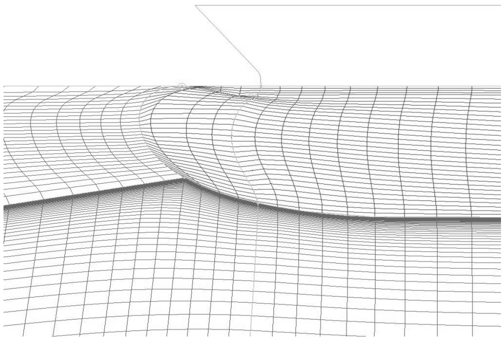

Fig. 4.19 Difficulty in Structured Grid Generation for Nose-Up Bulbous Bow of M.S. No.740

Therefore in the place of the NEPTUNE code, the SURF code [32] was used to calculate the form factors of the improved ship hulls with the nose-up bulbous bow at Rn=4×10^6. This code is based on an unstructured grid method for simulating three-dimensional incompressible viscous flows. The governing equations to be solved numerically are the Navier-Stokes equations with artificial compressibility. The spatial discretization is based on a finite volume method for an unstructured grid. Second order accuracy in space is achieved using a flux-difference-splitting scheme with the MUSCL approach for inviscid terms and a central difference scheme for viscous terms. Time integration is carried out by the backward Euler method. The linear system derived by the linearization in time is solved by the Gauss-Seidel iteration. For the analysis of high Reynolds number flows, the Spalart-Allmaras turbulence model is used. The turbulence equation is solved in a similar way as the Navier-Stokes equations.

For the grid generation, the structured grid was used for the most part of the computed region around the hull, while the unstructured grid was used for the region above the present bulbous bulb. Since some unfavorable skewness was found in the grids near the top of the bulb, the multi-block and the unstructured grids should be applied for this region. In the case of the high-bulb and the conventional one, the structured grid could be successfully applied. When the computation was made on the ship flow around the hull with free surface, the structured grid can be applied for as shown in **Fig. 4.20,** but it can give no favourable results by the double model flow method for the present ship hull.

On the other hand, in the case of the grid generation for the double model flow of M. S. No. 740 with the nose-up bulb, 5x5x97 tetrahedron cells for unstructured grids were partly used to generate the grid blocks between the full load waterline and the top of the bulb because the distance between the top of the bulb and the load water line was the order of 10^{-6} L_{PP}.

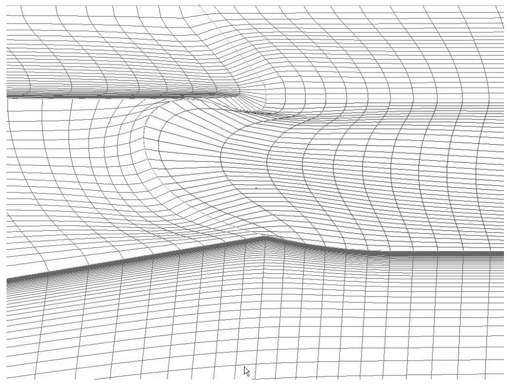

Fig. 4.20 Structured Grid Generation for Nose-Up Bulbous Bow of M.S. No.740 with Free Surface

The computational condition was the same as that for the NEPTUNE computation as described in the previous section 4.3.2 (2). The comparison of the form factors among five ship hulls is shown in **Fig. 4.21.** Except M. S. No.739, a qualitatively good agreement between the computations and experiments is observed. Most of the computational results are under-predicted by 0.025 for the ship hulls without the nose-up bulb. In order to obtain the form factor as a usual experimental procedure, the CFD computation was carried out at the low speed of Fn=0.06 but over-predicted by 0.025. In this computation, the converged solutions were not easily obtained. With the grid generation by the different block division, no remarkable difference in the computational results is found.

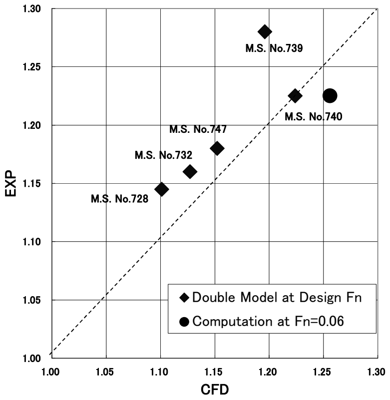

Fig. 4.21 Comparison of Form Factor between CFD Computations by SURF and Experiments

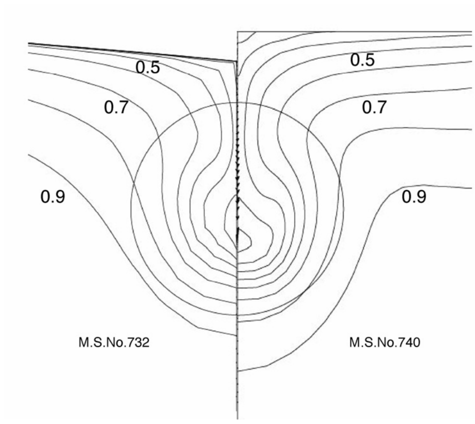

Fig. 4.22 Comparison of Computed Wake Distribution between M.S. No.732 and No. 740

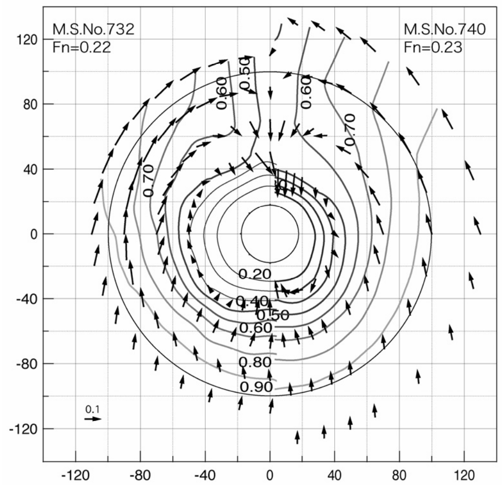

Fig. 4.23 Comparison of Measured Wake Distribution between M.S. No.732 and No. 740

The computed results of the wake distribution of the prototype hull, M. S. No. 732 and improved hull, M. S. No. 740 with the double model method are compared in **Fig. 4.22** at the propeller disk. Comparing with the experimental results on two ship models as shown in **Fig. 4.23**, the present CFD computation shows the characteristics of the wake distribution for each ship hull, concerning the center of wake, the width of wake peak.

4.3.3 Design of Propeller

In order to improve the cavitation performance of the designed propeller, the NMRI optimum propeller design method was applied for the design. First of all, the expanded area ratio a_E was determined to be 1.00 by using the Burrill's chart. As the blade section, modified NACA type was employed. The pitch distribution and camber line were determined by the lifting surface theory based on the Vortex Lattice Method (VLM) and by the Lerbs' optimum circulation distribution.

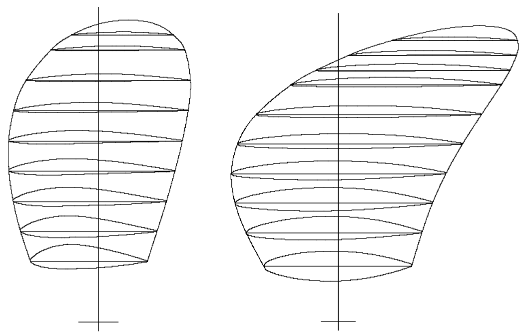

(a) Prototype　　(b) Improved Type

Fig. 4.24 Comparison of Propeller Geometry

For the designed propellers, 30-degree skew was applied to moderate the variation of unsteady cavity. The blade shapes of the prototype (M. P. No. 576) and improved propeller (M. P. No. 589) are shown in **Fig.4.24**. The principal particulars of tested propeller models are shown in **Table 4.5**.

Table 4.5 Principal Particulars of Tested Propellers

M.P. No.			576	577	589
Diameter (Full Scale)	D_{PS}	[m]	9.600		9.800
Diameter (Model)	D_{PM}	[m]	0.200		0.20417
Boss Ratio	x_B	[-]	0.1800		0.1875
Pitch Ratio at 0.7R	$P_{0.7}$	[-]	0.9300	0.9494	0.8959
Exp. Area Ratio	a_E	[-]	0.770	1.000	
Skew Angle	Θ_S	[deg]	10.0	13.0	28.10
Rake Angle	κ	[deg]	5.00		-3.00
Number of Blade	Z	[-]	6		

The propeller open water characteristics of prototype (M. P. No. 576 and 577) and the improved propeller (M. P. No. 589) models are shown in **Fig. 4.25**.

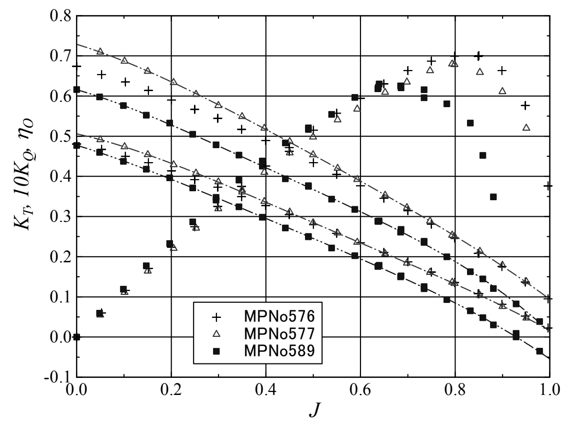

Fig. 4.25 Propeller Open Water Characteristics on Three Tested Propeller Models

4.3.4 Cavitation Performance

To confirm the design results, the cavitation experiments behind the complete ship model were performed.[33)]

(1) Wake Simulation

The wake simulation for the estimated full-scale wake was made with setting the appropriate position and using the suitable size of the flow liners.

The wake distribution of the improved ship model, M. S. No. 740 was measured at the 400m towing tank. The estimated wake by Sasajima-Tanaka method based on these measurements is shown in **Fig. 4.26**. Comparing with the estimated wake distribution of the prototype ship model, M. S. No. 732 as shown in **Fig. 4.4**, the wake becomes more uniform and the wake peak becomes lower from 0.5 to 0.4 roughly.

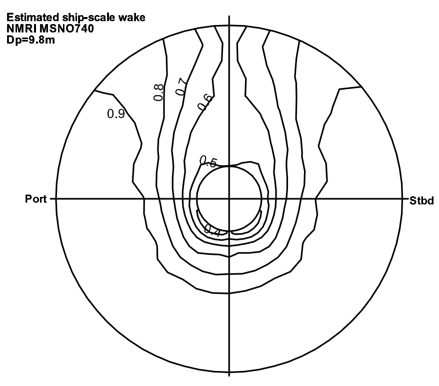

Fig. 4.26 Estimated Full-Scale Wake Distribution for Improved Ship (M. S. No. 740)

The comparison between simulated wake distribution and estimated one are shown in **Fig. 4.27**. It can be said that the wake simulation for this ship was made quite reasonably in the region where cavitation occurs and the propeller tip sweeps.

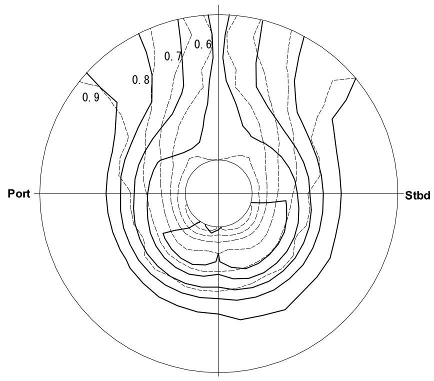

Fig. 4.27 Comparison between Target and Simulated Wake Distribution in the Cavitation Tunnel

(2) Experimental Condition

By using the self-propulsion test results, the powering was made on the designed propeller, M. P. No. 589 for the improved ship model. The experimental conditions at the MCR under the full load condition and at the NOR under the ballast condition are shown in **Table 4.6**.

Table 4.6 Experimental Condition

Condition		MCR (0.8R)	NOR (0.8R)
Engine Output		MCR	85%MCR
BHP (including 20% SM)	[MW]	95.0	80.7
	[PS]	129,105	109,739
Loading Condition		Full Load	Ballast
Thrust Loading Coefficient	C_T	1.056	1.218
Thrust Coefficient	K_T	0.1718	0.1840
Propeller Revolution Rate	N [rpm]	107.7	100.2
Cavitation Number	σ_N	0.884	0.801

(3) Cavitation Appearance

The cavitation observation was conducted on the designed propeller, M. P. No. 589. The cavitation extent on the improved propeller drastically decreases as shown in **Fig. 4.28**. The desinence of unsteady cavitation on the present propeller blades becomes gentler due to the adoption of skew and optimum geometrical shape.

On the designed propeller, slight face cavitation was observed. This face cavitation seems to be not detrimental due to very thin and incipient pattern, because the recent research reported that face cavitation is not always detrimental.[33), 35)] This suggests that the present design method should have a certain face margin for designing the propeller.

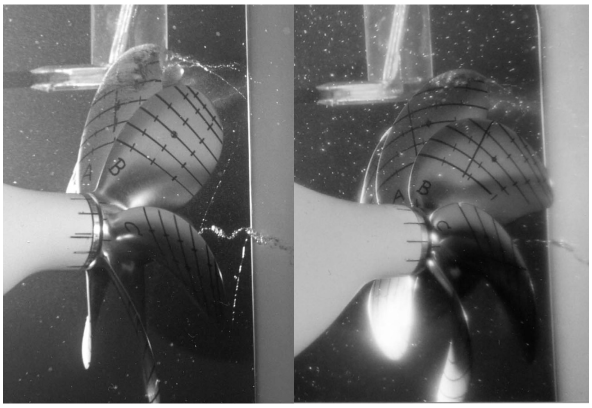

(a) Prototype(MP No.576) (b) Improved Type(MP No.589)
Fig. 4.28 Comparison of Cavitation Appearance behind Each Ship under MCR Condition ($\sigma_{N\_0.8R}$, Θ=20deg)

(4) Pressure Fluctuations

The pressure fluctuations were measured on the pressure gauges fitted to the hull surface above the propeller. The comparison of the pressure fluctuation amplitudes scaled up to full-scale at first, second and third blade rates among three designed propellers are shown in **Fig. 4.29**.

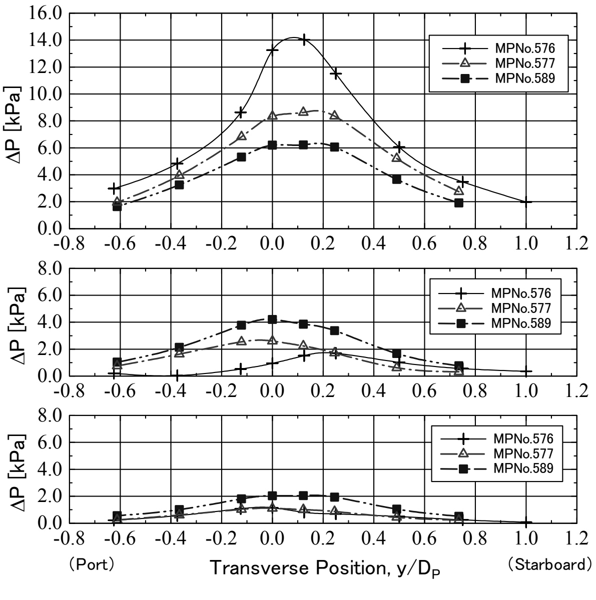

Fig. 4.29 Measured Pressure Fluctuation Amplitudes Induced by the Prototype and Improved Propellers Working behind the Improved Ship Model (M.S. No. 740)

The pressure fluctuation amplitude at the first blade rate of the improved propeller is 6kPa and in comfortable level, while the amplitude induced by the MAU propellers are 9kPa and 14kPa. Two of the latter are not acceptable for the propeller designers and ship builders. On the second and third blade rates of the improved propeller model, however, the pressure amplitudes become twice of those induced by the prototype propeller but they are acceptable.

The comparison of the pressure fluctuations between the full load and the ballast condition is shown in **Fig. 4.30**.

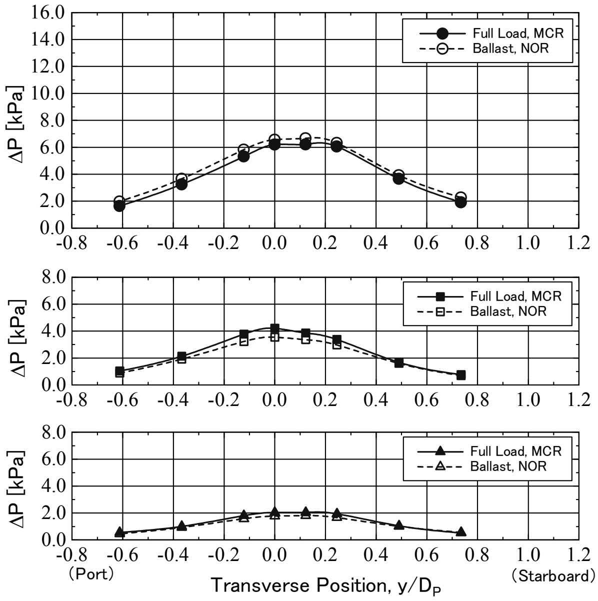

Fig. 4.30 Measured Pressure Fluctuation Amplitudes Induced by the Improved Propellers Working behind the Improved Ship Model (M.S. No. 740)

4.4 Final Ship Hull and Propeller

4.4.1 Design of Ship Hull

As described in the previous section, the wave resistance of the improved ship in the full load condition was sufficiently low, while that in the ballast condition was extremely high. Then, two hull forms were designed to reduce the wave resistance under the ballast condition within the marginal increase in the resistance under the full load condition by employing the SRC estimation method based on the Neural Network Technology. The principal particulars of the finally designed ship models are shown in **Table 4.7**

One of them, M. S. No. 747 has the nose-up bulbous bow and the other one, M. S. No. 750 has "high bulb" whose center is higher than the middle in height as those shown in **Fig. 4.2**.

In order to further reduce the pressure fluctuations induced by the propeller and cavitation, the stern shape of M. S. No. 747 was designed modifying that of the improved ship from M. S. No. 740 as shown in **Fig. 4.16** and that of M. S. No. 750 was not modified from M. S. No. 747. Both ship hulls have "semi tunnel stern" similar to that of M. S. No. 747 as shown in **Fig. 4.17**.

Table 4.7 Principal Particulars of Final Ships

Final Design Ship (Scale Ratio=48)			Full Scale Size	
			M.S. No.747	M.S. No.750
Bow Shape			Nose-Up Bulb	High Bulb
Stern Shape			Low Bulb+Semi Tunnel	
Length between P.P.	L_{PP}	[m]	344.00	
Length at Load Water Line	L_{WL}	[m]	344.74	
Breadth	B	[m]	55.50	
Draft (Design)	d_{Design}	[m]	13.00	
Draft (Scantling)	d_{Scant}	[m]	14.50	
Depth	D	[m]	29.00	
Propeller Shaft Height	H_{SC}	[m]	5.00	

4.4.2 Performance of Ship Hull

The resistance and self-propulsion tests were performed on two ship models. The form factors 1+k are 1.180 for M. S. No. 747 and 1.175 for M. S. No. 750 under the full load condition. The wave resistance coefficients $C_W x10^3$ are 0.303 for M. S. No. 747 and 0.213 for M. S. No. 750. Under the ballast condition, those are 0.443 for M. S. No. 747 and 0.331 for M. S. No. 750. Both resistance coefficients under the ballast condition are less than 0.777 for M. S. No. 740, while those under the full load condition becomes higher than 0.059 for M. S. No. 740. The predicted values of effective horsepower under the full load conditions are 70,308PS for M. S. No. 747 and 67,111PS for M. S. No. 750. Under the ballast (85% full load) condition, the effective horsepower for M. S. No. 750 is 67,334PS and drastically less than 69,271PS for M. S. No. 747 and 71,620PS for M. S. No. 740.

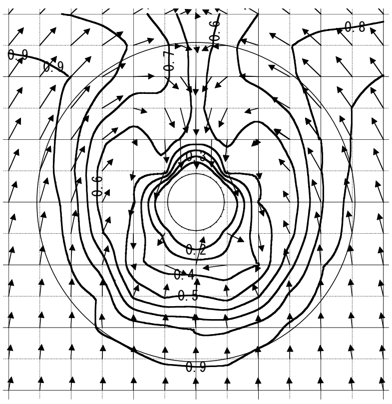

Fig. 4.31 Measured Wake Distribution behind M. S. No.747 at the 400m towing Tank

The self-propulsion factors under the full load condition, 1-t, $1\text{-}w_{TM}$, and η_R for M. S. No. 747 are 0.835, 0.677, 1.013, while those for M. S. No. 750 are 0.842, 0.676 and 1.010. No big differences in the self-propulsion factors are found. The predicted values of delivered horsepower are 103,648PS for M. S. No. 747 and 98,385PS for M. S. No. 750 under the full load conditions. These are 14.7% and 8.9% higher than 90,333PS for the improved ship, M. S. No. 740.

The wake measurements are performed at the 400m-towing tank on M. S. No. 747 and the measure results are shown in **Fig. 4.31**.

4.4.3 Design of Propeller

For the final ship with the installed engine of 100MW (135,900PSx106rpm), the propeller was designed at the NOR (85%MCR, 115,515PS) with the propeller revolution margin of 4%.[36] based on the powering results of M.S. No. 750.

The principal particulars of four designed propellers are shown in **Table 4.8** and their photos are shown in **Fig. 4.32**.

Table 4.8 Principal Particulars of Final Propellers

M.P. No.			600	601	602	603
Diameter (Full Scale)	D_{PS}	[m]	9.800			
Diameter (Model)	D_{PM}	[m]	0.20417			
Boss Ratio	x_B	[-]	0.1875			
Pitch Ratio at 0.7R	$P_{0.7}$	[-]	0.8909	0.9014	0.8450	0.8812
Exp. Area Ratio	a_E	[-]	1.000			0.900
Skew Angle	Θ_S	[deg]	28.10			28.00
Rake Angle	κ	[deg]	-1.29	-1.43	-3.00	2.60
Number of Blade	Z	[-]	6			

(1) M.P. No.600

This Propeller was designed by the NMRI optimum propeller design method for the averaged wake with Lerbs' optimum circulation distribution [37] in the same manner as the improved propeller, M. P. No. 589.

Several additional improvements were made. One is the utilization of the blade section with larger leading edge radius from 0.66%C to 1.10%C and another is the adoption of partial backward rake [38] to increase the face cavitation margin.

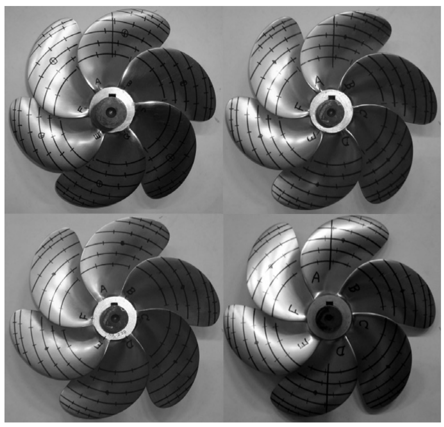

Fig. 4.32 Comparison of Blade Shape among Tested Propeller Models for the Final Design Ship

(2) M.P. No.601

This propeller was initially designed by the same manner as M. P. No. 600 but some novel design options were introduced.

Firstly, in order to increase the propeller efficiency, the radial load distribution and pitch distribution given by Lerbs' theory were increased near the tip of the propeller. By using the unsteady propeller lifting surface theory based on the Kernel Expansion Method (KEM) [20], the unsteady blade surface pressure distribution was computed during one revolution. The blade geometrical shape was modified as to minimize the summation of the squared tension pressure measured from vapor pressure. One of the blade modifications is to shift the center of the chordwise load distribution to the trailing edge.

(3) M.P. No.602

This propeller blade was designed by the geometrical optimization modifying the maximum point of chordwise camber distribution, the pitch and the maximum camber in the radial direction as the design parameters. As an optimization technique, the genetic algorithm was employed so as to maximize the propeller efficiency at the design point under the constrained condition that the cavitation extent is less than half of the basic propeller.

The geometrical shape, such as, skew, rake, blade width and the maximum thickness was kept the same as those of M. P. No. 600 and 601. For the computation of the propeller performance and the prediction of cavitation extent, one of the propeller lifting panel methods, "SQCM" developed by the Kyushu University [24] was utilized. The cavitation occurrence was judged when the representative surface pressure of each panel becomes less than the vapor pressure or

$$\sigma_N + C_{PN} < 0 .$$

(4) M.P. No.603

Using the non-linear propeller lifting surface theory [27], the pitch and camber distribution were determined to obtain an optimum blade surface load distribution. In order to increase the propeller efficiency, the blade area ratio was decreased from 1.0 to 0.9. To addition, 7-degree backward tip rake from $07R_O$ to the tip was adapted to reduce the pressure fluctuations.

4.4.4 Propeller Performance

The propeller open water tests were carried out on four designed propeller models in the NMRI No. 3 towing tank. The measured propeller open water characteristic curves are shown in **Fig. 4.33**. The Reynolds number defined by Kempf's definition is about 4.5×10^5 for M. P. No. 600 in the vicinity of the design point.

The comparison of the propeller efficiency among four propellers at the design thrust loading coefficient C_T of 1.059. The highest efficiency propeller is M. P. No. 603 and the second highest efficiency propeller is M. P. No. 602.

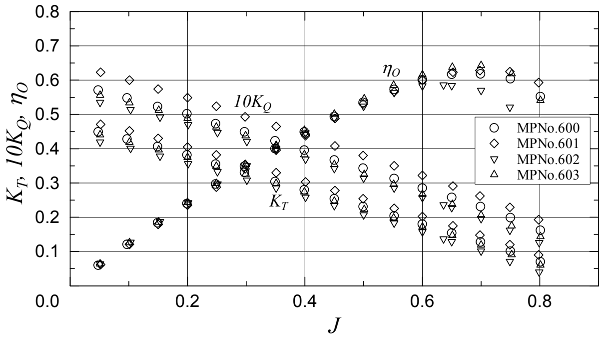

Fig. 4.33 Propeller Open Water Characteristic Curves on Designed Propeller Models for a Final Ship Hull

4.4.5 Cavitation Performance

(1) Wake simulation

The full-scale wake was estimated in the same manner as Sasajima-Tanaka's method described in the previous sections. The estimated full-scale wake simulation was made by the NMRI standard wake simulation method using the complete ship model, M. S. No. 747 together with the flow liners.

The finally simulated wake distribution is shown in **Fig. 4.34**. The wake distribution becomes wider than the target one.

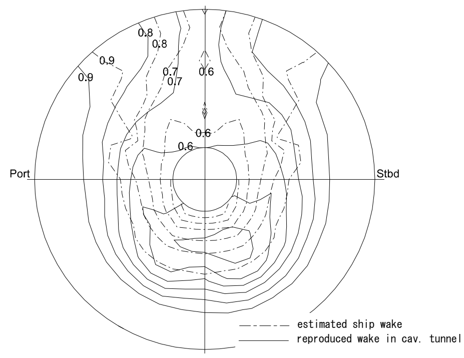

Fig. 4.34 Simulated Wake Distribution

(2) Experimental Condition

The cavitation test on M. P. No.600 was performed using M. S. No. 747 under three experimental conditions shown in **Table 4.9**. The measurement under the condition of the 85%MCR (NOR) and ballast load was omitted because both the thrust coefficient and cavitation number are almost similar to those under the condition of the MCR and the full load. In order to compare the cavitation performance of other three propellers with that of M. P. No. 600, the experimental condition was set to the same tested thrust coefficient K_T and cavitation number $\sigma_{n0.8R}$ for M. P. No. 600.

Table 4.9 Experimental Condition

Condition		MCR (0.8R)	MCR (S. C.)	NOR (0.8R)
Engine Output		MCR		85%MCR
BHP (including 20% SM)	[MW]	100.0		85.0
	[PS]	135,900		115,515
Loading Condition		Full Load	Ballast	Full Load
Thrust Loading Coefficient	C_T	1.082		1.059
Thrust Coefficient	K_T	0.166		0.165
Propeller Revolution Rate	N [rpm]	110.2		104.6
Cavitation Number	σ_N	0.884	0.749	0.936

(3) Cavitation Appearance

The cavitation extents among four propellers are shown in **Fig. 4.35**. The cavitation patterns on all of the tested propellers are sheet cavitation. The small sheet cavity occurs only around the tip except M. P. No. 602. Back sheet cavitation on M. P. No. 602 occurs from 0.4R to 0.6R due to the local higher pitch effect to match the thrust coefficient with the tested one. For all propeller models no face cavitation and no symptom of erosive cavitation were found.

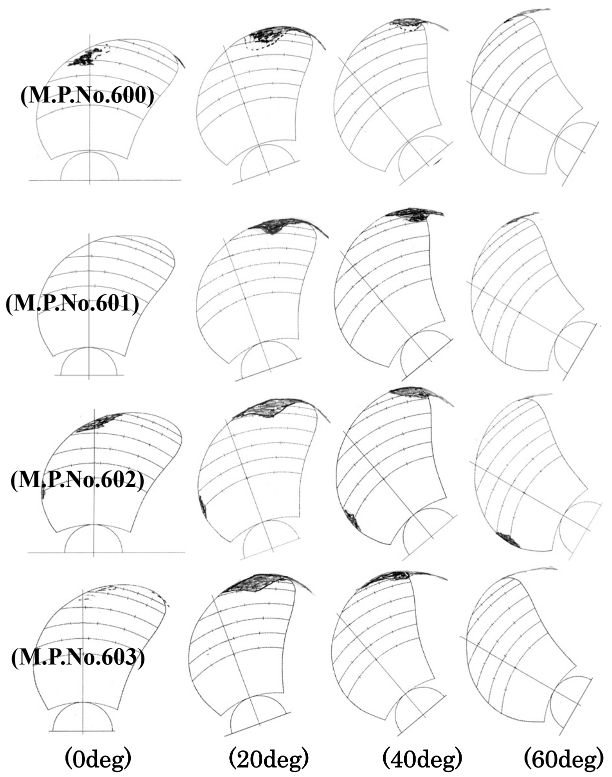

Fig. 4.35 Comparison of Cavitation Patterns among Four Designed Propellers

(4) Pressure Fluctuations

The arrangement of fourteen pressure gauges equipped with the hull surface of the complete ship model is shown in **Fig. 4.36**.

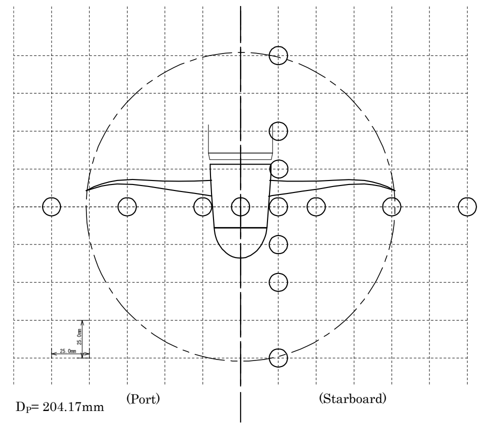

Fig. 4.36 Arrangement of Pressure Gauges

The comparison of the pressure fluctuation amplitudes at the first, the second and the third blade rates are demonstrated in **Fig. 4.37** on M. P. No. 600 under three experimental conditions. In this report, the measurement results are shown only in the transverse direction. The pressure fluctuation amplitudes at the first and the second blade rates under the ballast condition are the highest among three conditions but they are predicted only 2kPa in the full-scale ship.

(5) Discussions on the Propeller Design Results

The first propeller, M. P. No.600 was successfully designed along the aim in the design because no face cavitation was observed under all of experimental conditions and the obtained propeller efficiency is almost the same as the target one of 0.615.

The second propeller, M. P. No. 601 was designed, to increase the propeller efficiency due to the higher load distribution near the tip and to minimize the unsteady cavitation extent during one revolution. The obtained propeller efficiency is sufficiently high, while the pressure fluctuation amplitudes at each blade rate are the highest but less than the comfortable level.

The third propeller, M. P. No. 602 was designed to aim at the enhancement of propeller efficiency, while the efficiency of this propeller is the lowest among all tasted propellers. One of the reasons might be that the constraint condition which imposes less than half of the cavitation extent on the reference propeller, M. P. No. 602 is too strict to find more efficient solutions. The employed program code should be modified so that the code can offer a reasonable solution following to the variation of the camber lines in the searching process based on the genetic algorithm.

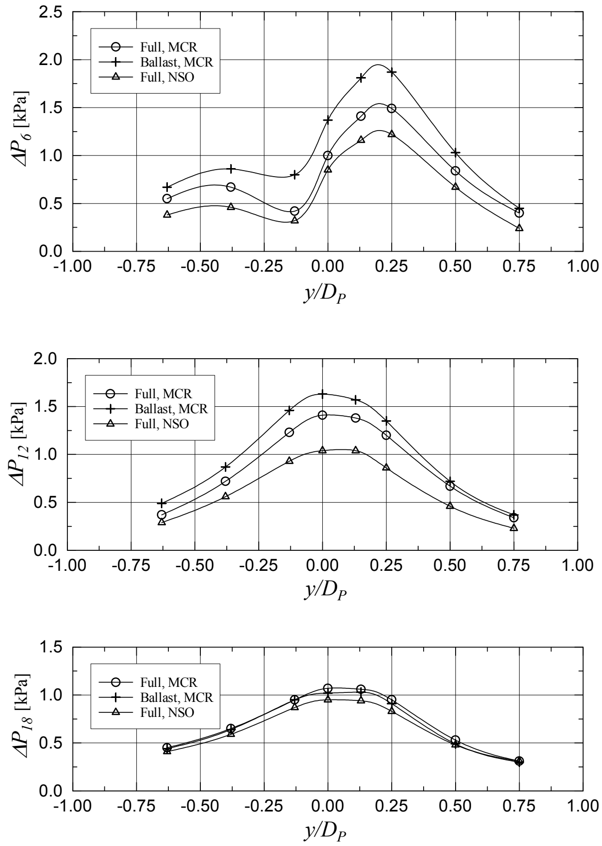

Fig. 4.37 Comparison of Pressure Fluctuation Amplitudes among Three Experimental Conditions for M. P. No.600

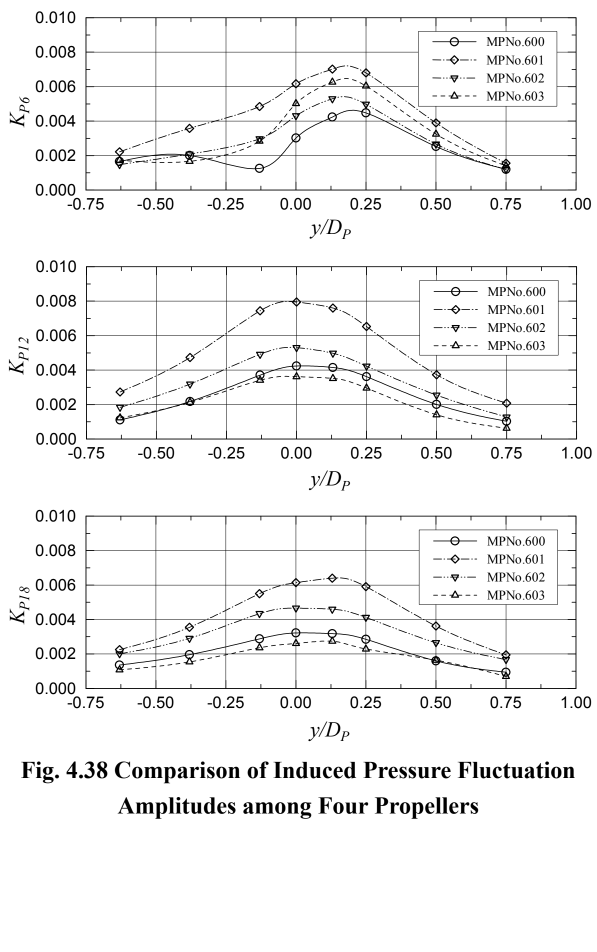

Fig. 4.38 Comparison of Induced Pressure Fluctuation Amplitudes among Four Propellers

The fourth propeller, M. P. No. 603 was designed to increase the propeller efficiency without the detrimental effects on erosion and pressure fluctuations. The propeller open water test shows that the propeller efficiency of the propeller is the highest due to the reduction of the expanded area ratio. The tip vortex cavitation of the present propeller is thin and then the second and the third orders of the pressure fluctuations are the lowest among all of the tested propellers. It can be said that the backward rake of the propellers is effective to reduce the pressure fluctuations, because the first order of the pressure fluctuations induced by the first propeller, M. P. No.600 with the backward rake is the lowest among all of the tested propellers. This result confirms the recent research that the backward rake reduces the effective pitch distribution.

4.5 Discussion on the Designed Ship Hull and Propeller

4.5.1 Improvement of Bow Shape

Several ship hulls were designed firstly to reduce the resistance or the effective horsepower aiming at the enhancement of propulsive performance of a high-powered ship.[41] The designed ship hulls including the prototype were examined through the resistance tests. Through the present design, the bow shape and the prismatic curve were modified to reduce the wave resistance. The SRC optimization method for the propulsive performance was employed for the optimization of the hull forms. Several kinds of bulbous bow were adopted, for example, the "nose-up bulb" and "high-bulb" as shown in **Fig. 4.2**. Concerning the nose-up bulbous bow, no papers on the experimental results have been published.

The models were manufactured without bilge keel to use the measured data for the validation of the NMRI CFD codes.

From the resistance tests on several ship models described in the previous sections, the wave resistance curve of the prototype ship with a normal bulb varies gently with the Froude number. On the other hand, the wave resistance around the design Froude number (Fn=0.22) becomes minimum and the bigger hump at the low Froude number (Fn=0.1) reveals. The determination of the form factor k for the ship hull with the nose-up bulbous bow is very difficult due to this effect.

Comparing with the full load condition, the present nose-up bulbous bow showed us the unfavorable effect that the wave resistance tremendously increase under the ballast and other conditions and higher than that with the normal bulbous bow. To adopt the nose-up bulbous bow, the ship hull should be designed not only at the design speed but also at the other ship speeds and loading conditions. It is expected that the CFD could accurately and speedily compute the ship resistance including the form factor, wake distribution, wave profile, wave breaking around the bow and the wave elevation around the transom stern.

4.5.2 Improvement of Stern Shape

In order to improve the propulsive performance, particularly the cavitation performance including pressure fluctuations, noise and erosion, the optimization of the stern shape is one of the most important issues to make the wake distribution as uniform as possible and to keep sufficient screw aperture.

The difficulty index DI proposed by the 23rd ITTC and shown in the section 3.4 is useful to design the stern shape. Since difficulty index in this formula, is proportional to the fifth power of the wake deficit Δw, it is one of the most predominant parameters. The wake deficit is defined by the difference between the maximum wake and the minimum wake. Therefore, the stern shape was improved to minimize the wake deficit defined by the difference between the maximum wake and the mean effective wake measured by the propeller model in the self-propulsion tests.

As one of the reasonable parameters to represent the wake uniformity, this report proposes the wake deficit given by the difference between the maximum effective wake w_{TMAX} and the effective mean wake w_T. The maximum effective wake should be determined around the angular position of zero degree, that is, the upright position in the outside of 50% radial position of the propeller. The comparison of wake deficit defined here, the tip clearance and difficulty index among three designed ships are shown in **Fig. 4.39**.

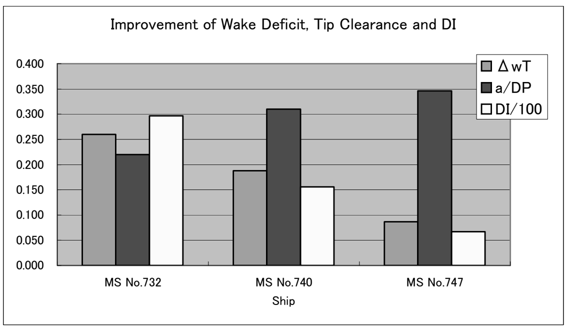

Fig. 4.39 Comparison of DI, Wake Deficit and Propeller Aperture among Three Ships

Three kinds of the stern shape designed for each ship is shown in **Fig. 4.16**. M. S. No. 732 is the prototype, M. S. No. 740 is the improved type and M. S. No. 747 is the final one. **Fig. 4.39** shows that the difficulty index becomes less than seven. If the wake deficit is less than 0.1 and the tip clearance is larger than around 0.35 D_P.

The comparison of the first, second and third blade rate of pressure fluctuation amplitudes among three ships is shown in **Fig. 4.40**. From the present measurements using M.S. No. 747, the pressure fluctuations are expected to become the minimum under the operating condition of the final ship estimated from the powering results on M. S. No. 750 whose stern shape is the same as M. S. No. 747.

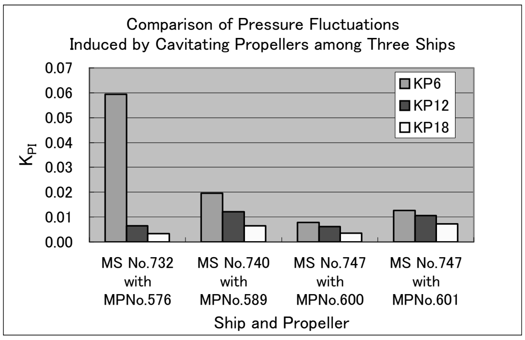

Fig. 4.40 Comparison of Pressure Fluctuations among Three Ships

5. Concluding Remarks

This report discusses the improvement of propulsive performance on a high-speed ship equipped with a high-powered propeller. The following condition can be drawn.

1. The nose-up bulbous bow drastically reduces the wave resistance of a large container ship under the design condition. The ship hull form with nose-up bulb, however, should be carefully designed considering other load conditions.
2. The reduction of wake deficit and the increase of screw aperture offer big reduction of pressure fluctuations induced by propeller and cavitation. This report shows the quantitative results based on the cavitation tests using the complete ship models.
3. The increase of wake uniformity reduces the propulsive efficiency. The trade-off in the design of ship hull is necessary to optimize the pressure fluctuations and propulsive performance.
4. The cavitation experiments show that the partial backward rake of propellers is effective to reduce cavitation and the pressure fluctuations without remarkable decrease in the propeller efficiency.

In this report, CFD computations were carried out on the designed large container ships. The difficulty in the present computations on the large container ships was found on the grid generation around the bulbous bow and the transom stern. Great efforts for the improvement are required to employ the CFD for designing this type of ship hulls as a reliable tool.

Acknowledgements

The review part of this report was written partly based on the data in "The Survey Report on Fundamental Research Tasks for Shipbuilding Technology, Investigation on Technical Research Tasks on High Speed – High Powered Propulsion System", entrusted by The Organization for Development of Shipbuilding Techniques of Japan and written by three of the authors.

The authors are grateful to all members of the 24th ITTC propulsion committee for their discussion, contribution and support in their activities. The authors also wish to express their gratitude to Mr. J. S. Carlton and Mr. P. A. Fitzsimmons (Lloyd's Register), and Mr. Jürgen Friesch and Mr. F. Mewis (HSVA) for their discussion and useful information.

Thanks are also due to the participants for 24th ITTC comparative computation on bearing forces of propeller working behind a large container ship, Prof. J. Ando (Kyusyu University), Dr. T. Hoshino (MHI), Dr. N. Ishii (MES), Dr. A. Mashiko (IHI), Dr. N. Sasaki (SHI in those day, NMRI at present), Dr. I.-H. Song and Dr. K.-J. Paik (Samsung), Dr. S. Yamasaki (Nakashima).

References (*; Written in Japanese)

1. Gallin, C. M., "Comparison of Propulsion Plants for Ultra Large Container Ships of Tomorrow", SNAME Transactions, Vol. 104, pp. 219～238 (1996)
2. Rosello, B. J. et. al., "An Efficient Single-Screw 11000TEU Container ship: The Suez Max SS", Marine Technology, Vol. 38, No. 4, SNAME, pp. 219～232 (2001.10)
3. Payer H. G., "Technological and Economic Implications of Mega Container Carriers", SNAME Transactions, Vol. 109, pp. 101～120 (2001)

4* Ikeda, Y., "History on Enlargement of Container Ship", Proc. of Symposium on Mega- Container Ship in Future, the Kansai Society of Naval Architects, Japan, pp. 2～10 (2001.6)

5* Wakiyama, N., "Over-Panamax Container Ship", Proc. of Symposium on Mega- Container Ship in Future, the Kansai Society of Naval Architects, Japan, pp. 47～59 (2001.6)

6* Sato, K., "Development on Contra-Rotating Propeller System for Large Container Ship - Preparing for 10,000TEU class", Proc. of Symposium on Mega- Container Ship in Future, the Kansai Society of Naval Architects, Japan, pp. 60～63 (2001.6)

7* Endo, M, "Ultra-Large Container Ships (ULCS)", Proc. of Symposium on Mega- Container Ship in Future, the Kansai Society of Naval Architects, Japan, pp. 64～76 (2001.6)

8. Carlton, J. S., "The Propulsion of Large Container Ship, a Note on the Propulsion Options", Boxship 2001, Annex to Ultra-Large Container Ships (2001. 5) or Proc. of Symposium on Mega- Container Ship in Future, the Kansai Society of Naval Architects, Japan, pp. 77～94 (2001.6)
9. Meyne, K. J. et. al., "The Development of the Propeller Design for the World's Largest Reefer Container Ships", Proc. of SNAME Symposium Propellers/Shafting 2000, Vol. 1, pp. 1～11 (2000.9)
10. The 23rd ITTC Propulsion Committee, "Final Report and Recommendations to the 23rd ITTC", Proc. of 23rd ITTC, Vol. 1, Venice, pp. 89～151 (2002.9)
11. Hämäläinen, R. et. al., "Hydrodynamic Development for a Large Fast Monohull Passenger Ferry", SNAME Transactions, Vol. 106, pp. 413～441 (1998)
12. The Propulsion Committee, "Final Report and Recommendations to the 24th ITTC", Proc. of 24th ITTC, Vol. 1, Edinburgh, pp. 73～136 (2005.9)
13. Mewis, F., Klug, H., "Very Large Container Ships Difficulties and Potential from the Hydrodynamic Standpoint", Proc. of International Symp. on Naval Architecture and Ocean Engineering, Shanghai, 3-1～3-19, (2003.9)

14* Ukon, Y., "Hydrodynamic Issues on a Mega Container Ship Propeller", Proc. of 4th Meeting on NMRI Research, Mitaka, pp. 171～174, (2004.7)

15. Kim, S.-E., Choi, S.-H., Veikonheimo, T., "Model Tests on Propulsion Systems for Ultra Large Container Vessel", Proc. of The 12th International Offshore and Polar Engineering Conference, Kitakyusyu, pp.520～524, (2002)
16. Kühmstedt, T., "Containers in the Air", Proc. of Design and Operation of Container Ships, the Royal Institution of Naval Architects, London, pp. 15～22, (2003.4)

17* Ukon, Y., Fujisawa, J., Kudo, T., "Reduction of Pressure Fluctuations Induced by Cavitating Propellers due to Air Injection through the Hull at the Stern of a Ship", Trans. of the West-Japan Society of Naval Architects, Vol. 99, pp. 33～42, (2000.3)

18. Holtrop, J., Valkhof, H., "The Design of Propellers and Developments in the Propulsion of Container Ships", Proc. of Design and Operation of Container Ships, the Royal Institution of Naval Architects, London, pp. 23～

30, (2003.4)
19* Kume, K., Ukon, Y., Fukasawa R., Fujisawa, J., Matsuda, N., "Experimental Evaluation Techniques on a Cavitating Propeller of a Mega-Container Ship in a Cavitation Tunnel", Proc. of 4th Meeting on NMRI Research, Mitaka, pp. 343～34, (2004.7)
20* Koyama, K., "Numerical Method for Propeller Lifting Surface in Non-Uniform Flow and Its Application", Journal of the Society of Naval Architects of Japan, Vol. 137, pp. 78-87, (1975. 6)
21* Hatano, S., Minakata, J., Yamasaki, S., "The Estimation of the Performance Characteristics of the Propeller by the Lifting Line and Lifting Surface Theory", Trans. of The West-Japan Society of Naval Architects, No. 49, pp. 177-220, (1975)
22 Hoshino, T., Nakamura, N., "Propeller Design and Analysis Based on Numerical Lifting-Surface Calculations", Proc. of the 2nd International Conference on Computer Aid Design, Manufacture and Operation in the Marine and Offshore Industries (CDADMO'88), Southampton, (1988. 9), pp. 549-574
23 Chao, K.-Y., Streckwall, H., "Berechnung der Propellerumströmung mit einer Vortex-Lattice Methode", Jahrbuch Schiffbautechnischen Gesellschaft, Band 83, (1989)
24 Ando, J., Maita, S., Nakatake, K., "A New Surface Panel Method to Predict Steady and Unsteady Characteristics of Marine Propeller", Proc. of 22nd Symposium on Naval Hydrodynamics, (1998), pp. 142-154.
25 Ishii, N, "Prediction of Propeller Performance and Cavitation Based on the Numerical Modeling of Propeller Vortex System", Proc. of International Symposium on Propulsor and Cavitation, Hamburg, (1992), pp. 33-41.
26 Lee. C.-S., "Prediction of steady and unsteady performance of marine propeller with or without cavitation by numerical lifting-surface theory", Ph. D. Thesis, MIT (1979)
27 Mori, M., Katagiri, T., Ochi, M, "Computer Program for Propeller Design and Examples of Application", IHI Engineering Review, Vol. 7, No.2, (1974)
28* Kanai, T., "Application of the Neural Network to Estimate of Ship's Propulsive Performance and Hull Form Optimization", Proc. of Trans. of the West-Japan Society of Naval Architects, No. 99, (2000.3)
29* Takeshi, H., et. al., "Ship Flow Computation on a Series of Mega-Container Hull Forms by CFD", Proc. of 5th Meeting on NMRI Research, Mitaka, pp. 353～354, (2005.6)
30* Takeshi, H., et. al., "Grid Generation and CFD Analysis of large Breadth/Draft Hull Forms with Nose-Up Bulbous Bow", Proc. of 6th Meeting on NMRI Research, Mitaka, pp. 181～182, (2006.7)
31 Hirata, N., et. al., "An Efficient Algorithm for Simulating Free-Surface Turbulent Flows around an Advancing Ship", Journal the Society of Naval Architects, Japan, Vol. 185, pp. 1～8 (1999.6)
32 Hino T., "Navier-Stokes Computations of Ship Flows on Unstructured Grids", Proc. of the 22nd Symp. on Naval Hydro., Washington D.C, (1998)
33* Kume, K., et. al., "Cavitation Test for Improved Propellers toward a Mega-Container Ship", Proc. of 5th Meeting on NMRI Research, Mitaka, pp. 329～322, (2005.6)
34 Göran Bark, et al., "Cavitation Erosion on Ship Propeller and Rudder", Proc. of 9th Symposium on Practical Design of Ships and Other Floating Structures, Lübeck, pp. 554～561 (2004)
35 The Specialist Committee on Cavitation Erosion on Propellers and Appendages on High Powered/High Speed Ships, "Final Report and Recommendations to the 24th ITTC", Proc. of 24th ITTC, Vol. 2, Edinburgh, pp. 509～542 (2005.9)
36* Kume, K., et. al., "Propeller Design and Cavitation Characteristics on a Single-Screw Very large Container Ship", Conference Proceedings the Japan Society of Naval Architects and Ocean Engineers, Vol. 2, pp. 131～134, (2006.5)
37 Lerbs, H. W., "Moderately Loaded Propellers with a Finite Number of Blades and Arbitrary Distribution of Circulation", Trans. SNAME, Vol.60, pp.73 ～ 117, (1952.11)
38* Yamasaki, S., et. al., "Cavitation Test of a Forward skewed Propeller and Partial Rake Propeller", Proc. of Conference Proceedings the Japan Society of Naval Architects and Ocean Engineers, Vol. 1, pp. 253～256 (2005.12)
39* Ando, J., et. al., "A Simple Surface Panel Method to Predict Steady Marine Propeller Performance", Proc. of Journal the Society of Naval Architects, Japan, Vol. 178, pp. 61～69 (1995.12)
40* Yamasaki, S., "A Numerical Method for Non-Linear Steady Propeller Lifting Surface and Its Application for Highly Skewed Propeller Design" Trans. of the West-Japan Society of Naval Architects, Vol. 62, pp. 47～68, (1981.8)
41* Ukon, Y., et. al., "Enhancement of Propulsive Performance for High-Speed Ships with a High-Powered Propeller", Proc. of 6th Meeting on NMRI Research, Mitaka, pp. 189～190, (2006.7)